Article

Neuron

Excitatory Cerebellar Nucleocortical Circuit Provides Internal Amplification during Associative Conditioning

Highlights

- Cerebellar nuclei provide modular corollary discharge to the cerebellar cortex
- Nucleocortical afferents have unique molecular and ultrastructural features
- Eyeblink conditioning induces structural plasticity of nucleocortical mossy fibers
- Nucleocortical afferents amplify the amplitude of conditioned eyeblink responses

Authors

Zhenyu Gao, Martina Proietti-Onori, Zhanmin Lin, ..., Tom J.H. Ruigrok, Freek E. Hoebeek, Chris I. De Zeeuw

Correspondence

z.gao@erasmusmc.nl (Z.G.), c.dezeeuw@erasmusmc.nl (C.I.D.Z.)

In Brief

The role of the closed-loop circuitry between cerebellar nuclei and cortex is unknown. Gao et al. show that nucleocortical inputs provide corollary discharges to the granular layer, are plastic upon eyeblink conditioning, and amplify the amplitude of conditioned responses.

Gao et al., 2016, Neuron *89*, 645–657
February 3, 2016
http://dx.doi.org/10.1016/j.neuron.2016.01.008

CellPress

Neuron
Article

Excitatory Cerebellar Nucleocortical Circuit Provides Internal Amplification during Associative Conditioning

Zhenyu Gao,[1,*] Martina Proietti-Onori,[1] Zhanmin Lin,[1] Michiel M. ten Brinke,[1] Henk-Jan Boele,[1] Jan-Willem Potters,[1] Tom J.H. Ruigrok,[1] Freek E. Hoebeek,[1] and Chris I. De Zeeuw[1,2,*]
[1]Department of Neuroscience, Erasmus MC, 3015 CN Rotterdam, the Netherlands
[2]Netherlands Institute for Neuroscience, Royal Dutch Academy of Arts & Sciences (KNAW), 1105 BA Amsterdam, the Netherlands
*Correspondence: z.gao@erasmusmc.nl (Z.G.), c.dezeeuw@erasmusmc.nl (C.I.D.Z.)
http://dx.doi.org/10.1016/j.neuron.2016.01.008

SUMMARY

Closed-loop circuitries between cortical and subcortical regions can facilitate precision of output patterns, but the role of such networks in the cerebellum remains to be elucidated. Here, we characterize the role of internal feedback from the cerebellar nuclei to the cerebellar cortex in classical eyeblink conditioning. We find that excitatory output neurons in the interposed nucleus provide efference-copy signals via mossy fibers to the cerebellar cortical zones that belong to the same module, triggering monosynaptic responses in granule and Golgi cells and indirectly inhibiting Purkinje cells. Upon conditioning, the local density of nucleocortical mossy fiber terminals significantly increases. Optogenetic activation and inhibition of nucleocortical fibers in conditioned animals increases and decreases the amplitude of learned eyeblink responses, respectively. Our data show that the excitatory nucleocortical closed-loop circuitry of the cerebellum relays a corollary discharge of premotor signals and suggests an amplifying role of this circuitry in controlling associative motor learning.

INTRODUCTION

Accurate execution and error correction of motor behavior requires specific neural computation and dedicated wiring of neural circuits in the brain. Cortical and subcortical regions are usually connected by closed-loop circuitries, which are thought to determine the precision of final output patterns (Ahissar and Kleinfeld, 2003; Kelly and Strick, 2003; McCormick et al., 2015; Moser et al., 2008; Shepherd, 2013; Strick et al., 2009). The cerebellum controls a variety of sensorimotor tasks with high spatial and temporal accuracy (De Zeeuw et al., 2011; Dean et al., 2010; Gao et al., 2012; Ito, 2006), but surprisingly little is known about its internal closed-loop circuitry between the cerebellar nuclei and cortex. The cerebellar cortex receives glutamatergic climbing fiber (CF) and mossy fiber (MF) inputs from inferior olive and other pre-cerebellar nuclei, respectively, while the cerebellar nuclei receive axon collaterals of the same CF and MF inputs (Voogd and Ruigrok, 1997). In the cerebellar cortex, CF and MF signals ultimately converge onto GABAergic Purkinje cells (PC), which in turn project to the cerebellar nuclei, forming the main output unit of the cerebellum.

In current learning theories on cerebellar function, the CFs are thought to relay sensory error signals and provide an external feedback to the molecular layer of the cerebellar cortex during motor learning (Cerminara and Apps, 2011; De Zeeuw et al., 2011; Dean et al., 2010; Steuber and Jaeger, 2013; Voogd and Ruigrok, 1997). In contrast to models of other cortical and subcortical circuits in the brain (Ahissar and Kleinfeld, 2003; Alexander et al., 1986; McCormick et al., 2015; Nicolelis and Fanselow, 2002; Pennartz et al., 2009), it is unknown whether internal feedback mechanisms from the cerebellar nuclei onto the cerebellar cortex may also facilitate adaptive sensorimotor processing (Ankri et al., 2015; Houck and Person, 2015). In principle, cerebellar internal corollary discharges relaying an efference copy of motor signals as a feedback can be advantageous for control of movements, because preparations and predictions for new movements can be initiated ultrafast, long before sensory feedback from the periphery is provided (Hallett and Lightstone, 1976; Perrone and Krauzlis, 2008; Sperry, 1950).

In this study, we sought to examine the potential role of cerebellar nucleocortical projections (Dietrichs and Walberg, 1980; Gould and Graybiel, 1976; Hámori et al., 1981; Houck and Person, 2015; Tolbert et al., 1978; Trott et al., 1998; Umetani, 1990) as an internal corollary feedback to the granular layer during Pavlovian eyeblink conditioning (Boele et al., 2010; Gonzalez-Joekes and Schreurs, 2012; Krupa and Thompson, 1997; Morcuende et al., 2002). During eyeblink conditioning, a conditional stimulus (CS), such as a tone or light, is repeatedly paired with an unconditional stimulus (US), such as an air-puff to the eye, at a fixed inter-stimulus interval of several hundred milliseconds so as to produce a conditioned response (CR) (Medina et al., 2000, 2002). So far, studies aimed at unraveling the mechanisms underlying

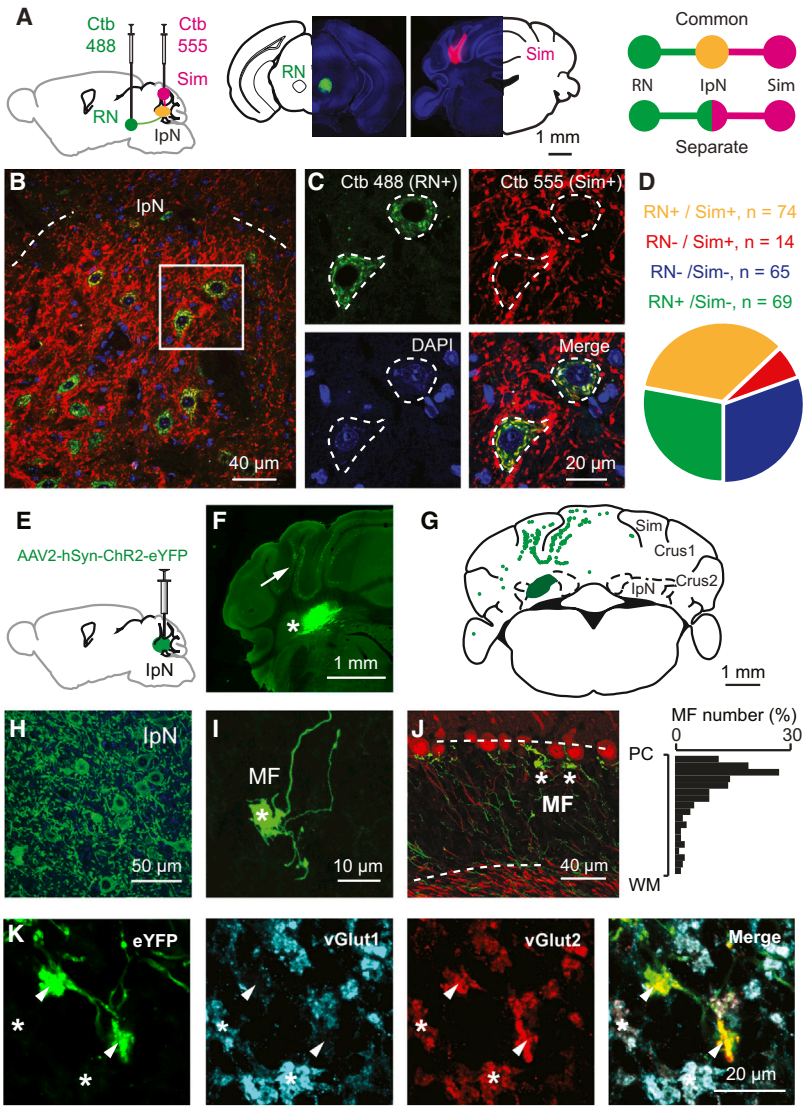

Figure 1. Nucleocortical Projections from the Cerebellar Interposed Nucleus

(A) Scheme and example of experimental setup showing retrograde labeling of IpN neurons following injection of Ctb tracers in the RN and lobule simplex (Sim). The rationale of the experimental setup is to illustrate the common (yellow) or separate (green and red) IpN neurons that project to RN and Sim (right).

(B) Example image of an IpN region with labeling from RN (Ctb 488, green) and Sim (Ctb 555, red).

(C) High-magnification images showing co-labeled IpN neurons.

(D) Summary chart of the retrogradely labeled neurons in IpN.

(E) Schematic showing viral injection of AAV2-hSyn-ChR2-eYFP into the left interposed nucleus.

(F) Example of AAV infected IpN (asterisk) and nucleocortical projections (arrow).

(G) Distribution of nucleocortical MF rosettes in a coronal cerebellar section.

(H and I) eYFP expressing IpN neurons (H) and nucleocortical MF projection (I) with enlarged rosette and filopodia-like structure. Asterisk indicates an MF rosette.

(J) Example (left) and summary (right, N = 3) of the nucleocortical MF (asterisks) distribution in the granular layer (between dashed lines), PCs are labeled in red.

(K) Nucleocortical MFs that express vGlut2, but not vGlut1 (arrowheads). Note the surrounding MF rosettes (asterisks) that are positive for both vGlut1 and vGlut2.

RESULTS

Morphological Features of Nucleocortical Fibers in Eyeblink Region

Since the main motor route of the eyeblink paradigm is mediated by the deeper part of the primary fissure in the lobule simplex (HVI), interposed nuclei (IpN), and red nucleus (RN) (Boele et al., 2010; Gonzalez-Joekes and Schreurs, 2012; Krupa and Thompson, 1997; Morcuende et al., 2002), we first investigated to what extent the nucleocortical pathway from IpN neurons to the lobule simplex indeed provides an efference copy of the signals forwarded to the RN (Ruigrok and Teune, 2014). The retrograde tracers Ctb Alexa Fluor 555 and Ctb Alexa Fluor 488 were injected into the mouse cerebellar lobule simplex (HVI) and corresponding contralateral RN, respectively (N = 4). In the IpN areas where both tracers converged, we found that 52% (74/143) of the RN projecting neurons showed nucleocortical labeling and 84% (74/88) of the nucleocortical projecting neurons projected to the RN (Figures 1A–1D and S1). These data indicate that a substantial part of the nucleocortical afferents in the lobule simplex relays efference copy signals of the presumptively excitatory IpN neurons that project to the RN (De Zeeuw and Ruigrok, 1994). Next, to establish the morphology and identity of the terminals of the nucleocortical afferents in the lobule simplex, we injected AAV particles coding for eYFP-tagged channelrhodopsin 2 (AAV2-hSyn-ChR2-eYFP) into the IpN and found prominent

the acquisition of this form of associative learning have focused mainly on the role of cerebellar cortical processes in the molecular layer, including long-term depression and long-term potentiation of the parallel fiber to PC synapse (Aiba et al., 1994; Ito et al., 2014; Schonewille et al., 2010, 2011; Welsh et al., 2005) and intrinsic plasticity of PCs (Johansson et al., 2014; Schonewille et al., 2010), most of which probably depend on the presence or absence of external feedback provided by the CFs (Gao et al., 2012; ten Brinke et al., 2015). Here, we establish that the excitatory input from the cerebellar nuclei to the cerebellar cortical eyeblink region strengthens the conditioned eyeblink response by providing an internal amplification loop, highlighting the emerging concept that the mechanisms underlying motor learning are distributed across various parts of the cerebellar modules and include an internal closed-loop circuitry (Casellato et al., 2015; Gao et al., 2012; ten Brinke et al., 2015).

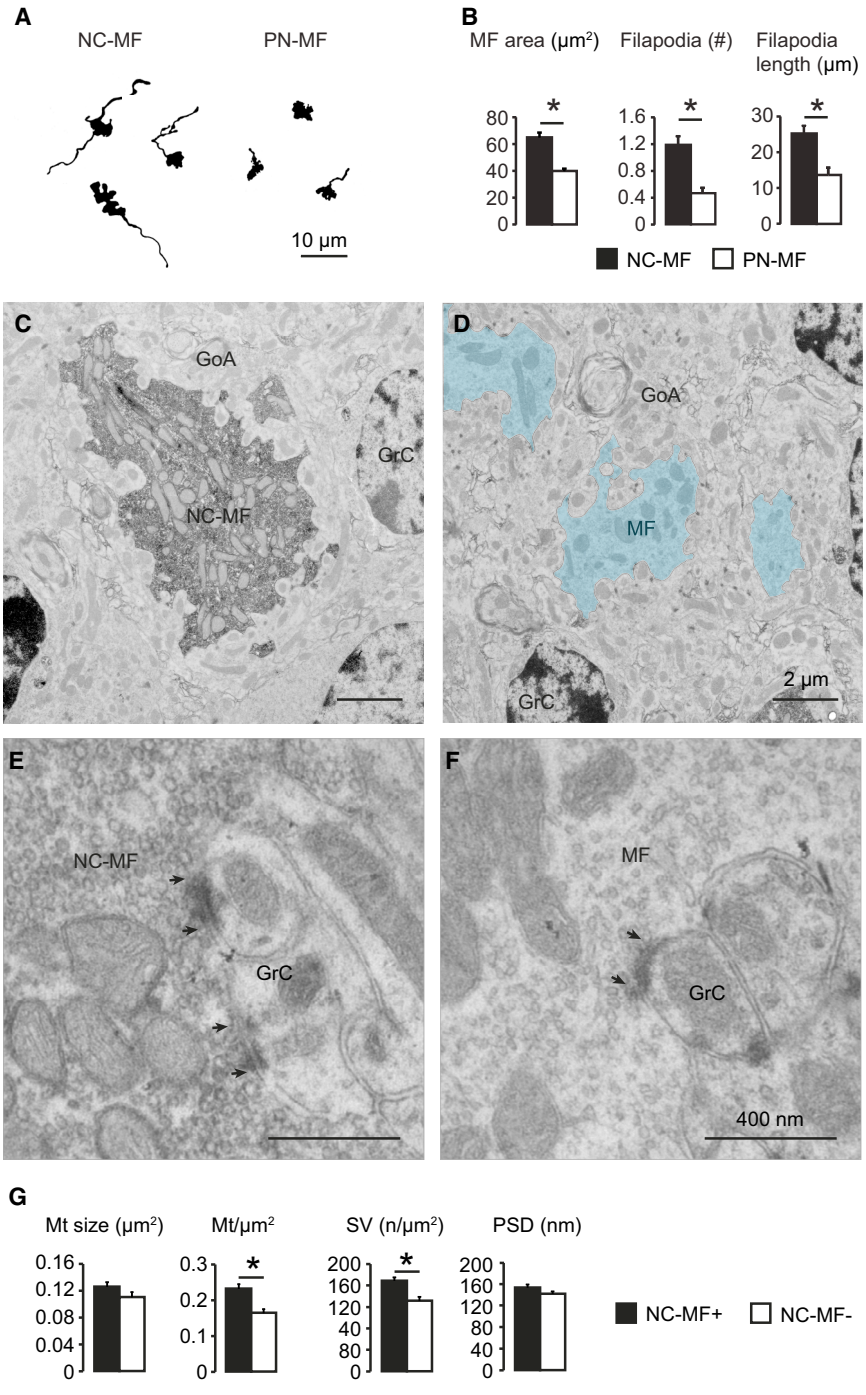

Figure 2. Morphological Characteristics of Nucleocortical Mossy Fibers

(A) Examples of nucleocortical MFs (NC-MF) and pontine nucleus MFs (PN-MF) labeled with anterograde tracer BDA 10,000 Da.

(B) Quantitative comparison of the morphology of the nucleocortical MFs (NC-MF, n = 34) and MFs originating from the pontine nuclei (PN-MF, n = 31). The NC-MFs have a larger size, higher number of filopodia per rosette, and longer filopodia length (all $p < 0.05$).

(C–F) Electron micrographs of a NC-MF terminal and adjacent unlabeled MF (granule cells: GrC and Golgi cell axon: GoA).

(G) The synaptic densities are indicated with double arrows. The NC-MF (n = 17) has a higher density of mitochondria ($p = 0.04$) and synaptic vesicles ($p = 0.002$), compared with adjacent unlabeled MFs (n = 21) (mitochondria: Mt, synaptic vesicle: SV, postsynaptic density: PSD) (*$p < 0.05$). The data show mean ± SE.

axonal labeling within and outside of cerebellum (Figures 1E–1J and S2). Within the cerebellar cortex, axonal terminals were found predominantly in the ipsilateral paravermal and hemispheric areas including the lobule simplex, Crus 1, Crus 2, paramedian lobule, and copula pyramidis (Figures 1G and 1I). Less dense projections were found in ipsilateral (para)flocculus and contralateral vermal and paravermal regions (Figures 1G and S2; Table S1). The nucleocortical fiber terminals formed large rosettes with filopodia-like protrusions, manifesting the MF rosette. Notably, these MF terminals preferentially targeted the superficial granular layer (Figure 1J). In addition, the nucleocortical MFs expressed exclusively presynaptic glutamate transporter vGlut2, whereas the majority of surrounding pre-cerebellar MF rosettes expressed both vGlut1 and vGlut2 (Gebre et al., 2012; Hioki et al., 2003) (Figure 1K). When we compared the morphology of the nucleocortical MF with the pre-cerebellar MF rosettes originating from the pontine nuclei, we found that the nucleocortical MF rosettes had a larger diameter as well as more and longer filopodia-like structures compared with pre-cerebellar MFs from pontine nuclei (Figures 2A and 2B). At the ultrastructural level, nucleocortical MF terminals contained higher densities of mitochondria and synaptic vesicles compared with neighboring, unlabeled MF rosettes, whereas the size of mitochondria and length of post-synaptic density (PSDs) did not differ (Figures 2C–2G). These data highlight a prominent projection of nucleocortical MFs with unique molecular and morphological features and suggest that they carry an efference copy signal of cerebellar premotor output commands.

The organization of the olivocerebellar system is characterized by repetitive parasagittal circuits, commonly acknowledged as cerebellar modules (Apps and Hawkes, 2009; Voogd and Ruigrok, 1997). To find out whether nucleocortical MFs involved in eyeblink conditioning form an internal feedback circuitry within the borders of the relevant module, we studied the MF distribution in mice with AAV2-hSyn-ChR2-eYFP injections in the

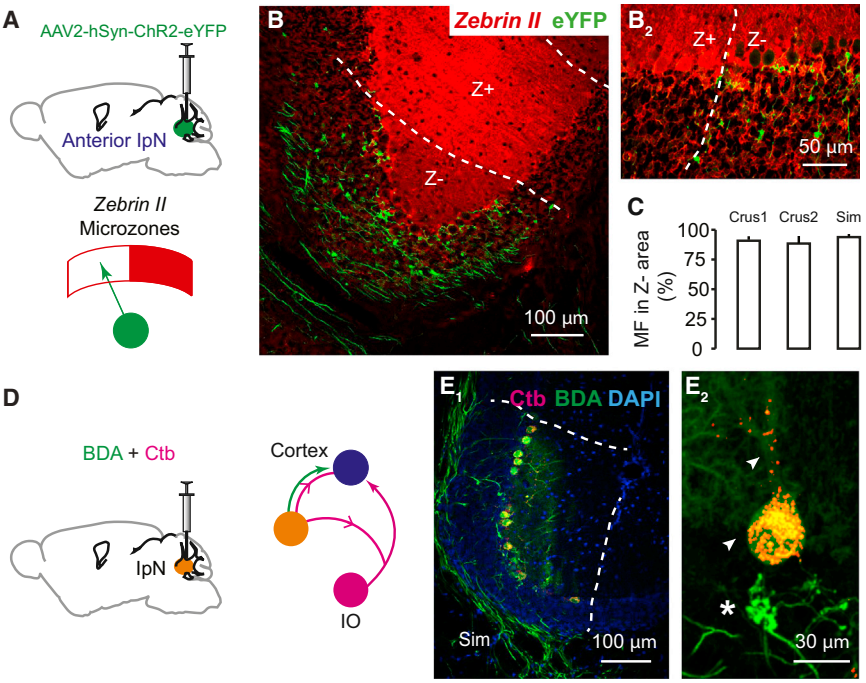

Figure 3. Modular Organization of Nucleocortical Projections

(A) Experimental setup to investigate the relation between nucleocortical afferents and zonal marker *Zebrin II*.

(B) Distribution of nucleocortical MF (green) in relation to *Zebrin II* (red) expression at the trough of the simplex lobule (B1) and the border between *Zebrin II* positive (Z+) and negative (Z−) zones in Crus 1 (B2).

(C) Quantification of the nucleocortical MF terminating at the Z− zones in Crus 1 (90.5% ± 3.3%), Crus 2 (88.5% ± 6.2%), and the lobule simplex (93.7 ± 2.8%), N = 4.

(D) Experimental setup to investigate relation of nucleocortical afferents and CF zones. The arrowheads indicate the tracing directions.

(E) BDA 10,000 Da and Ctb 555 injection in the anterior IpN labeled cortical modules (between dashed lines) in the lobule simplex (Sim) (E1). Nucleocortical MF and PC are co-localized in the same module (E2). The PC soma and adjacent CF were labeled with CTb (yellow, arrowheads), and the nucleocortical MF was labeled with BDA (green, asterisk). The data show mean ± SE.

anterior IpN, a region connected with cerebellar modules negative for marker *Zebrin II* (Sugihara, 2011; Voogd and Glickstein, 1998). In line with the eyeblink regions identified in rabbit (Attwell et al., 1999; Mostofi et al., 2010), we observed that nucleocortical MFs of these animals were found predominantly in regions negative for *Zebrin II*, including the trough of the lobule simplex (Figures 3A–3C). More specifically, we observed that 90.5% (±3.3%), 88.5% (±6.2%), and 93.7% (±2.8%) of the nucleocortical MF originating in the anterior IpN terminated in the *Zebrin* negative zones of Crus 1, Crus 2, and the lobule simplex, respectively. This finding, which implies a modular organization of the nucleocortical pathway, was further supported by the alignment of anterogradely labeled nucleocortical MFs with retrogradely labeled PC somata and CF terminals in the same region following co-injection of Biotin Dextran Amine 10,000 Da (BDA, for nucleocortical MF labeling) and Ctb Alexa Fluor 555 (for PC soma and CF terminal labeling) into a small area of the anterior IpN (Figures 3D and 3E). These data indicate that the regions that receive common nucleocortical MF projection also share the same CF projection and *Zebrin II* identity, consistent with the modular organization hypothesis of cerebellar functioning (Apps and Hawkes, 2009; Pijpers et al., 2006).

Electrophysiological Properties of Nucleocortical Fibers in Eyeblink Region

To further characterize the cellular properties of nucleocortical IpN neurons, we studied their morphological and electrophysiological properties in vitro (Figures 4 and 5). When we performed intracellular labeling following whole cell recordings of the large neurons of IpN, we found that the morphology of neurons with cerebellar cortical projections did not differ from the general population of excitatory cerebellar nuclei neurons (Aizenman et al., 2003; Uusisaari et al., 2007) in that they showed a similar soma size and number of primary dendrites (all p values > 0.31; Table S2). In addition, the electrophysiological properties of the nucleocortical cells were indistinguishable from the IpN neurons without any detectable projection to the cerebellar cortex (Table S2). Next, we characterized the electrophysiological properties of nucleocortical neurons at the level of their terminals in vitro with direct patch-clamp recordings of MF rosettes. Nucleocortical MFs labeled with eYFP could be readily visualized following injections of AAV-hSyn-ChR2-eYFP in the IpN (Figures 1E, 1F, and 4A). The rosettes showed the electrophysiological characteristics stereotypical of MFs (Rancz et al., 2007), including a small capacitance, high input resistance, and a hyperpolarization sag (Figure 4B; Table S3). Prolonged depolarization induced only a short burst of action potential firing and a subsequent steady depolarization block. Interestingly, we observed tonic spontaneous action potential firing in 4 out of 19 recorded MF rosettes (Figure 4C; Table S3). This activity probably reflects an intact connection to the cell body in the IpN within the slice (Figure 5), because we did not observe any silent MF terminal that showed tonic action potential firing in response to continuous depolarization. Applying repetitive current pulses up to 500 Hz at the nucleocortical rosettes resulted in reliable action potential firing (Figure 4D) with little adaptation in peak amplitudes, indicating that nucleocortical MFs can sustain reliable firing at extremely high frequencies, comparable to the high fidelity transmission of pre-cerebellar MFs encoding sensory information (Chabrol et al., 2015; Rancz et al., 2007; Ritzau-Jost et al., 2014; Saviane and Silver, 2006).

To identify the cortical neurons that receive direct nucleocortical MF input from IpN, we drove action potential firing specifically in the ChR2-expressing MF rosettes using optogenetics. Individual action potential firing could be reliably controlled

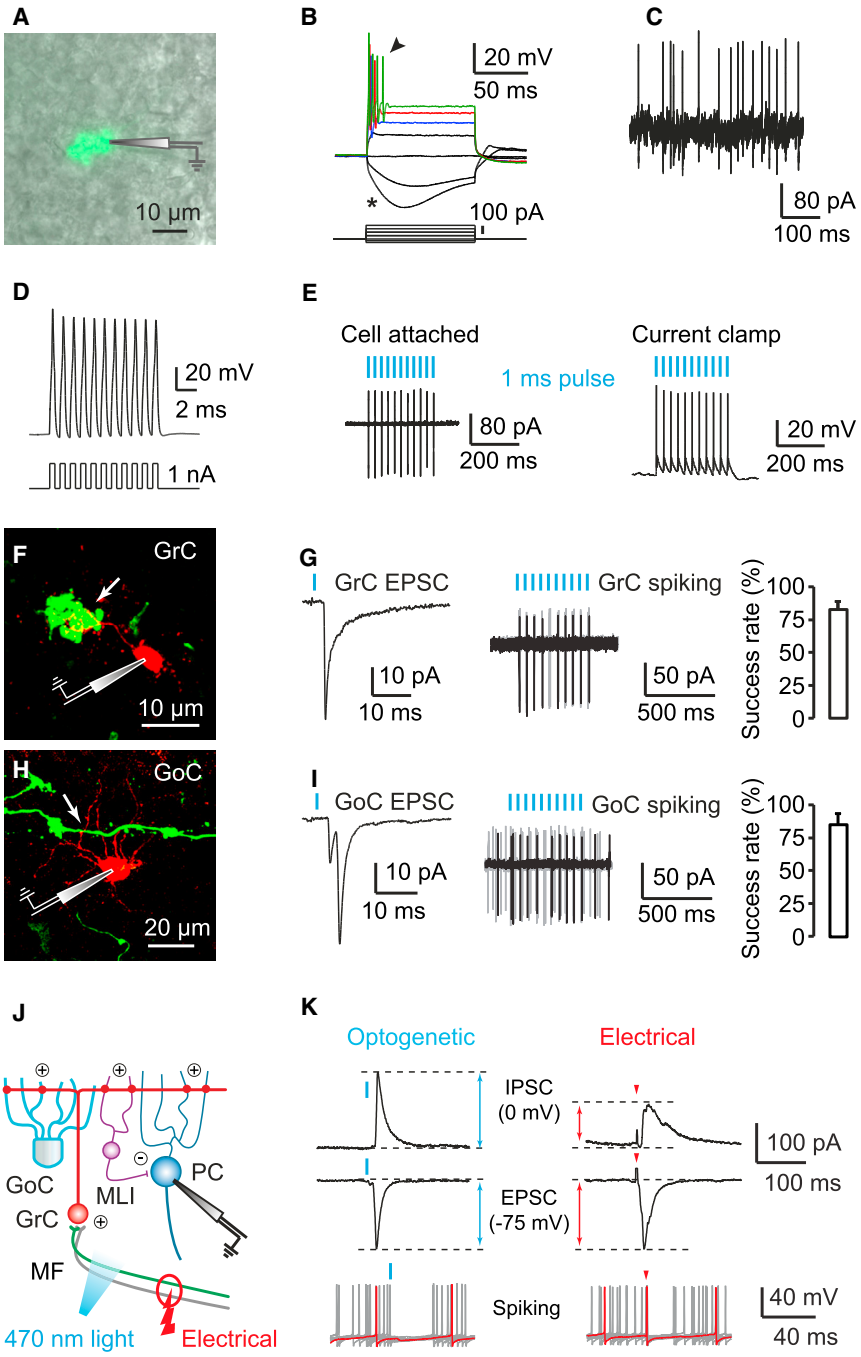

Figure 4. Nucleocortical Projection Imposes Unique Closed-Loop Circuit with Internal Feedback Properties

(A) Patch-clamp recording of an eYFP labeled MF rosette visualized by overlaying epifluorescence and DIC images.

(B) MF rosettes show current rectification, hyperpolarization sag (asterisk), and action potential firing (arrowhead) in response to steady-state current injections.

(C) Cell attached recording from a spontaneously firing nucleocortical MF.

(D) Repetitive current pulses drive MF rosette to fire robustly at 500 Hz with little adaptation in the action potential amplitudes.

(E) Optogenetic activation of a nucleocortical MF. The individual action potentials can be elicited with high temporal precision by a train of light pulses (1 ms 470 nm light at 30 Hz) in both cell attached and current-clamp modes.

(F) Nucleocortical MF (green) innervates granule cell dendrite (GrC, red, arrow).

(G) Whole cell recording of GrC-EPSC (left) and loose cell attached recording of GrC action potential firing (right) in response to 1 ms photo activation of NC-MF. We found a high success rate of inducing action potential firing in the GrC (81.7% ± 6.0% and n = 10).

(H) Nucleocortical MF (green) innervates Golgi cell dendrite (GoC, red, arrow).

(I) Whole cell recording of GoC-EPSC (left) and loose cell attached recording of GoC action potential firing (right) in response to 1 ms photo activation of NC-MF. We found a high success rate of inducing action potential firing in the GoC (83.8% ± 8.3% and n = 5).

(J) Experimental setup of identifying I/E ratio of PC responses. The GrC axon excites (+) the MLIs and PCs and the MLI in turn inhibits (−) the PCs. The ChR2 expressing nucleocortical MFs (green) are selectively activated by optogenetic stimulation, while a bundle of MFs with heterogeneous sites of origin (green and gray) are activated by electrical stimulation.

(K) Whole cell voltage clamp recordings of EPSC and IPSC elicited by optogenetic or electrical stimulation. The EPSC and IPSC components were isolated by clamping the PC at −75 mV and 0 mV, respectively. The higher IPSC to EPSC ratio (I/E ratio) from nucleocortical MFs circuits was found in PCs, compared with electrical stimulation (top). The optogenetic activation induces longer suppression of action potential firing compared with electrical stimulation (bottom). The data show mean ± SE.

with blue light pulses (470 nm, 1.2 mW, 1 ms pulse, onset latency 2.4 ± 0.2 ms, and n = 10; Figure 4E). We then recorded synaptic responses of neurons in the granular layer using optogenetic stimulation. Robust short latency monosynaptic excitatory post-synaptic currents (EPSCs) were found in both granule cells (GrCs, n = 13) and Golgi cells (GoCs, n = 9) (Figures 4F–4I and S3). In addition, feedforward excitatory inputs from the MF-GrC-GoC pathway were detected in GoCs (Figures 4I and S3). To further test the efficiency of eliciting action potential firing in GrCs and GoCs following nucleocortical stimulation, we performed extra-cellular loose cell attached recordings, avoiding the potential changes in cellular excitability that can occur in the whole cell mode. Optogenetic stimulation was sufficient to entrain well-timed action potential firing in both GrCs and GoCs with high success rates (Figures 4G and 4I). These results indicate that nucleocortical MFs originating in IpN can act as a robust and positive internal feedback to neurons in the lobule simplex in that they are configured to

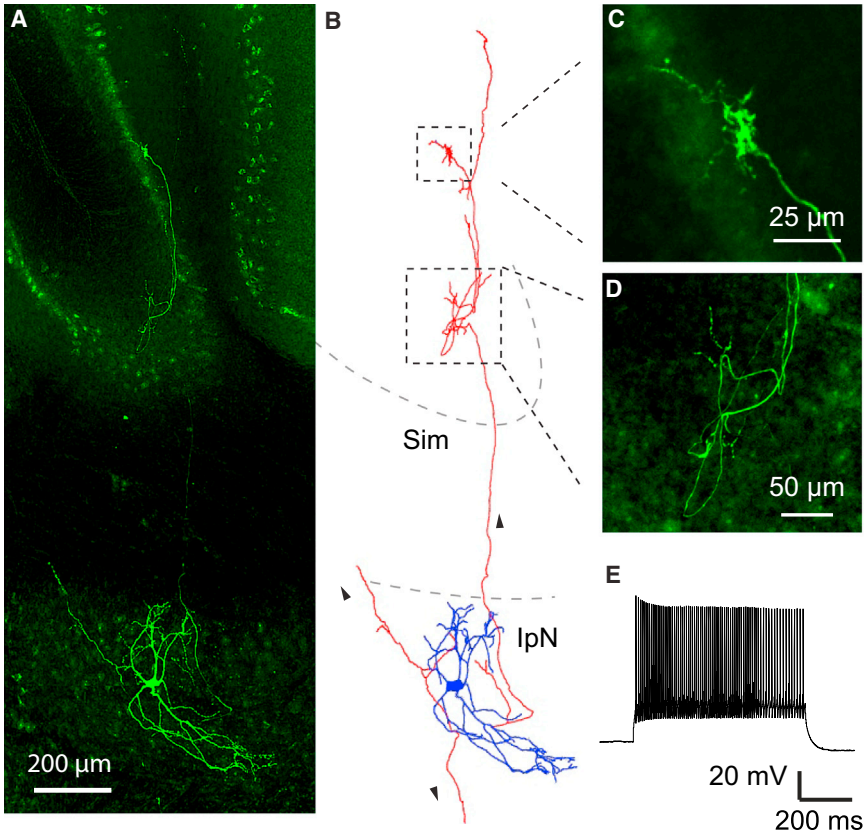

Figure 5. Physiologically Identified Cerebellar Interposed Nucleus Neuron Providing a Nucleocortical Projection

(A) Confocal image of an identified nucleocortical projecting IpN neuron recorded in vitro. The neuron was labeled with biocytin in the patch clamping pipette and visualized with fluorescent streptavidin Alexa Fluor 488.

(B) Neurolucida reconstruction of a labeled neuron shows an intact nucleocortical projection in the same sagittal plane. The arrowheads indicate the directions of extra-cerebellar and nucleocortical axonal projections (interposed nucleus: IpN and lobule simplex: Sim).

(C) Image of a nucleocortical MF rosette and accompanying filopodia-like structures.

(D) Image of *en passant* fiber and boutons from the same neuron.

(E) Example trace of action potential firing in response to 500 pA current injection in the neuron.

faithfully transmit action potential firing patterns to its granular layer.

MF afferents can control the activity of PCs via the local cerebellar cortical circuitry comprising GrCs, GoCs, and molecular layer interneurons (MLIs); they can either excite PCs via direct GrC-PC connections or inhibit PCs via feedforward GrC-MLI-PC processing (Figure 4J). To assess the relative contribution of these two inputs (D'Angelo and De Zeeuw, 2009), we compared the inhibition/excitation (I/E) ratio of the responses of individual PCs following selective optogenetic activation of nucleocortical MF afferents with that following local electrical activation of the complete mixed group of MFs, including both nucleocortical MFs and pre-cerebellar MFs. When the amplitudes of the excitatory components (i.e., EPSCs) were adjusted so as to be similar in the optogenetic and electrical stimulation paradigm (Figure 4K), we observed a greater inhibitory component (i.e., IPSC) in the PC response to nucleocortical MF activation, resulting in a greater I/E ratio (1.09 ± 0.06 with optogenetic stimulation versus 0.61 ± 0.09 with electrical stimulation; six pairs, $p = 0.006$, and paired Student's t tests). Consistent with this observation, all PCs showed longer simple spike suppression upon selective activation of nucleocortical MFs (pause duration with optogenetics 71.8 ± 10.5 ms, with electrical stimulation 58.4 ± 8.5 ms; six pairs; $p = 0.008$, and paired Student's t tests) (Figure 4K). Thus, in effect, nucleocortical MFs convey a strong inhibitory input onto PCs, even though they directly excite GrCs.

Structural Plasticity of Nucleocortical Fibers upon Eyeblink Conditioning

Although structural plasticity of MFs and their collaterals does not appear to be prominent following generally enriched, but non-associative, stimulation (Boele et al., 2013; Rylkova et al., 2015), it does occur during several sensorimotor learning tasks in which multiple stimuli are associated in a time-locked fashion (Boele et al., 2013; Ruediger et al., 2011). The high density of filopodia-like structures in the lobule simplex (Figures 2A and 2B) suggests that structural plasticity of the filopodia of nucleocortical MFs might also be involved in eyeblink conditioning, similar to what has been reported for extra-cerebellar MFs during other incremental learning paradigms (Ruediger et al., 2011). We first examined whether filopodia of nucleocortical MFs can in principle establish functional synapses. MF filopodial boutons labeled with eYFP consistently co-localized with vGlut2-positive endings (Figure 6A), indicating the presence of glutamatergic synapses at these sites. On average, 44.6 ± 10.5 vGlut2-positive boutons were associated with a single nucleocortical MF rosette. To identify whether these boutons contact Golgi cells, we injected AAV encoding red marker mCherry into the IpN of the GlyT2-eGFP mice, in which the majority of Golgi cells are labeled (Zeilhofer et al., 2005). Indeed, part of the vGlut2-positive boutons was found to contact Golgi cell dendrites (Figure S4). Next, we examined the ultrastructure of filopodial boutons. By combining serial sectioning with pre-embedding immuno-labeling of the tracer BDA (10,000 Da) and post-embedding immuno-gold labeling of GABA (see Experimental Procedures), we identified 18 filopodial boutons in two mice (Figures 6B–6D). Clear synaptic contacts were found in all 18 boutons, among which 15 contacted GrC dendrites (Figure 6C) and three contacted GoC dendrites as indicated by immuno-gold labeling (Figures 6D and S4). These data indicate that

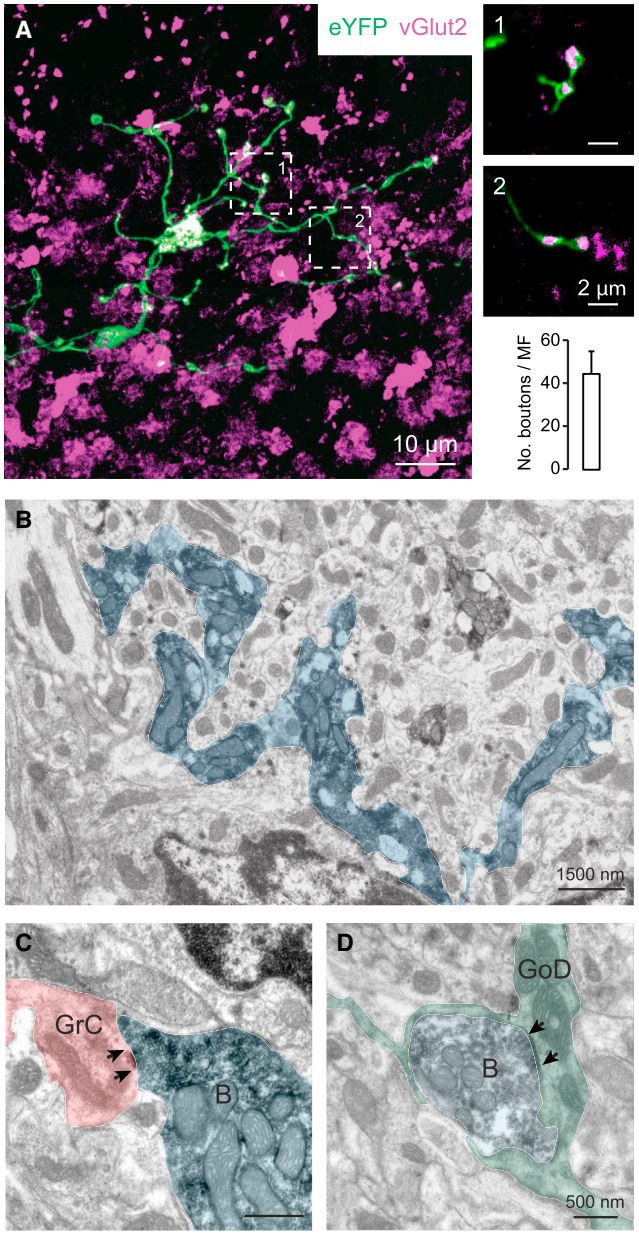

Figure 6. Filopodial Boutons Form Functional Synapses with Granule and Golgi Cells

(A) Representative image of a nucleocortical MF with filopodial protrusions. The insets 1 and 2 show vGlut2 positive filopodial boutons. The bar chart shows the average number of vGlut2 positive filopodial boutons per MF rosette.

(B–D) Representative electron microscopy (EM) image of BDA labeled filopodia traversing through the granule cell layer. The typical MF synaptic boutons (B) onto granule cell (GrC) and Golgi cell dendrites (GoD) are shown in (C) and (D), the arrows indicate PSD.

filopodial boutons can establish direct synaptic contacts with granule cells and Golgi cells.

We next set out to investigate whether these filopodia can undergo structural modification following eyeblink conditioning. Mice were trained to blink their eyes in a well-timed response to a light cue (CS) so as to avoid an air-puff to the eye (US) that was presented 250 ms after CS onset (Heiney et al., 2014) (Figure 7A). The density of filopodia boutons originating from nucleocortical MFs in the deeper lobule simplex of well-trained mice was significantly increased by 69.8% ($p = 0.001$) compared with that in naive mice (Figures 7C and 7D). In contrast, the length of the filopodia of nucleocortical MFs was significantly reduced ($p = 0.007$) (Figure 7D). This eyeblink training paradigm had no effect on the strength of nucleocortical MF synapses onto individual GrCs ($p = 0.7$), but further increased the I/E ratio in PCs ($p = 0.02$) (Figures 7E and 7F), indicating a preferential enhancement of the feedforward inhibitory GrC-MLI-PC pathway. These data point toward hard-wired plasticity of nucleocortical MFs during associative conditioning and suggest a novel function for these afferents providing an internal feedback, triggering larger numbers of specific sets of GrCs.

Nucleocortical Fibers Can Amplify Conditioned Eyeblink Responses

Since simple spike suppression can be quantitatively correlated with the amplitude of conditioned eyeblink responses (ten Brinke et al., 2015), we next set out experiments to find out whether direct and selective activation of nucleocortical MFs is sufficient to enhance conditioned eyeblink responses. We therefore trained a group of mice in which ChR2 was expressed in their nucleocortical MFs and in which an optic cannula was implanted superficially in the lobule simplex (Figure 8A). Once the mice showed a consistent conditioned eyeblink response (see Supplemental Information), we started optogenetic stimulation (for 10 ms coinciding with the CS onset) while recording the eyeblink responses as well as extra-cellular activity of the cerebellar nuclei and cerebellar cortex. The light intensity of the stimulus was adjusted for each mouse to make sure that it did *not* induce: (1) an instantaneous increase of action potential firing in the recorded cerebellar nuclei neurons; (2) an instantaneous eyeblink response; and (3) a detectable alteration of locomotion (Figure S5). Optogenetic activation of nucleocortical MFs at the onset of the CS enhanced the amplitude and shortened the onset-latency of the conditioned eyeblink responses ($p = 0.0008$ and $p = 0.005$, respectively; $N = 7$; Figure 8B). In contrast, in naive mice, optogenetic stimulation with maximum light intensity did not induce conditioned eyeblink responses (Figure S5), indicating that for the eyeblink conditioning paradigm, the nucleocortical loop could serve as a gain amplifier of the learned CS response. Importantly, the optogenetic stimulation confirmed an increased action potential firing ($p = 0.001$) of putative MLIs (Badura et al., 2013) and decreased simple spike firing ($p = 0.04$) in the majority of PCs in the lobule simplex (Figures 8C and 8D) in vivo, consistent with the GrC activation of MLIs and predominant feedforward inhibition onto PCs following nucleocortical activation, described above, as well as with the general changes in firing frequency of these neurons during eyeblink conditioning (ten Brinke et al., 2015).

If nucleocortical MFs contribute to eyeblink conditioning by providing internal amplification signals to the granular layer, one should also be able to quantify this contribution by acutely blocking these signals. We therefore tested another group of

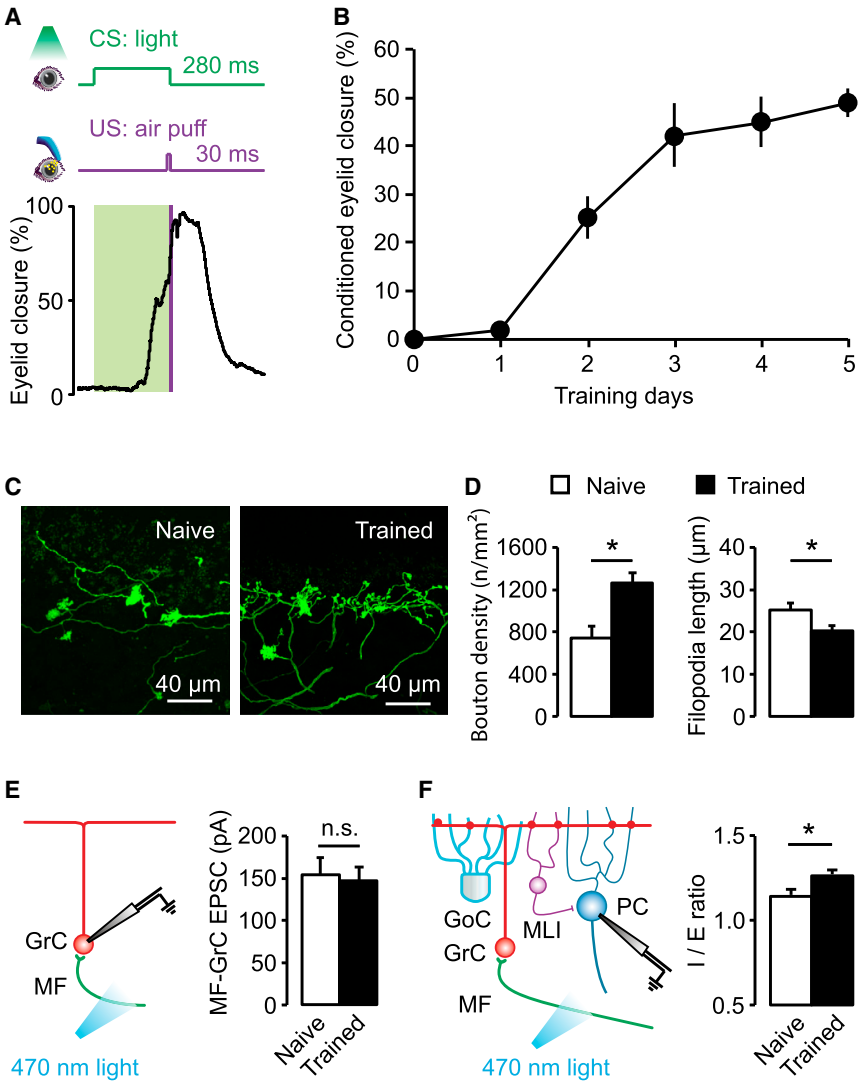

Figure 7. Plastic Changes in Wiring of Nucleocortical MF Filopodia Can Be Associated with Eyeblink Conditioning

(A) Scheme of eyeblink conditioning paradigm and representative trace of eyelid position in a conditioned mouse. The CS and US indicate conditional stimulus and unconditional stimulus, respectively.

(B) Development of conditioned eyeblink responses over 5 training days (N = 9).

(C) Example images of nucleocortical MFs (NC-MFs) in lobule simplex (HVI) of naive and trained mice.

(D) Filopodial boutons in trained mice (N = 9) show a higher local density, yet a shorter length, compared with those in naive mice (N = 8).

(E) Summary of EPSC peak amplitudes at the nucleocortical MF to GrC synapses in naive and eyeblink conditioning trained mice (naive, N = 9 and trained, N = 10).

(F) The feedforward I/E ratio was enhanced in the PCs of trained mice (naive 1.14 ± 0.03 and n = 28 and trained 1.26 ± 0.02 and n = 20). The data show mean ± SE (*p < 0.05).

trained mice, in which the inhibitory opsin, archaerhodopsin (eArch3.0), was virally expressed in IpN neurons. Dampening the activity of their nucleocortical MFs optogenetically for 250 ms with amber light (590 nm) in the lobule simplex at CS onset resulted in a significant reduction by 32% ± 3% in the amplitude of the conditioned eyeblink response (p = 0.003 and N = 5; Figure 8E). Instead, dampening nucleocortical MF activity without a CS did not induce an apparent eyeblink response or any other obvious type of motor behavior (Figure S5), making it unlikely that the optogenetically ChR2-driven behavioral effects described above resulted from antidromic effects in nucleocortical MFs.

DISCUSSION

The main findings of our study indicate that activity of the nucleocortical MF projection in the cerebellum contributes to gain control of learned eyeblink responses by providing internal amplification signals of an excitatory corollary discharge to the granular layer, which in turn is converted into PC inhibition via activation of MLIs. These findings corroborate the concept that increases in MLI activity and suppression of simple spikes correlate strongly with the amplitude of conditioned eyeblink responses (ten Brinke et al., 2015). Thereby, we establish for the first time a functional role for internal feedback of a corollary discharge from the cerebellar nuclei to the cerebellar cortex. To date, implications of such feedback signals have also been described in models of other major networks in sensorimotor control, such as cerebral cortex, superior colliculus, striatum, and spinal cord (Hantman and Jessell, 2010; Kalinovsky et al., 2011; Sommer and Wurtz, 2008). In general, feedback of corollary discharge can facilitate the prediction of sensory consequences of movements and improve learning and preparation of movements (Crapse and Sommer, 2008; Requarth and Sawtell, 2014). For models on cerebellar learning, this fast internal feedback mediated by MFs may complement the external feedback provided by the CF system (Cerminara and Apps, 2011; Llinás, 2011; Voogd and Glickstein, 1998), which is slower, but better designed to reset the phase and onset of motor programs in the modules (De Zeeuw et al., 2011; ten Brinke et al., 2015; Yarom and Cohen, 2002). Indeed, since both the MF and CF systems operate within the settings of the olivocerebellar modules, together they present a rich and complementary, computational repertoire to coordinate motor learning (Figure 9). For instance, the fast internal feedback loop appears well designed to amplify the amplitude of CRs directly after the movement is initiated, whereas the external loop may reset the motor cycle and speed up the onset of subsequent trials (De Zeeuw and ten Brinke, 2015; Welsh, 2002).

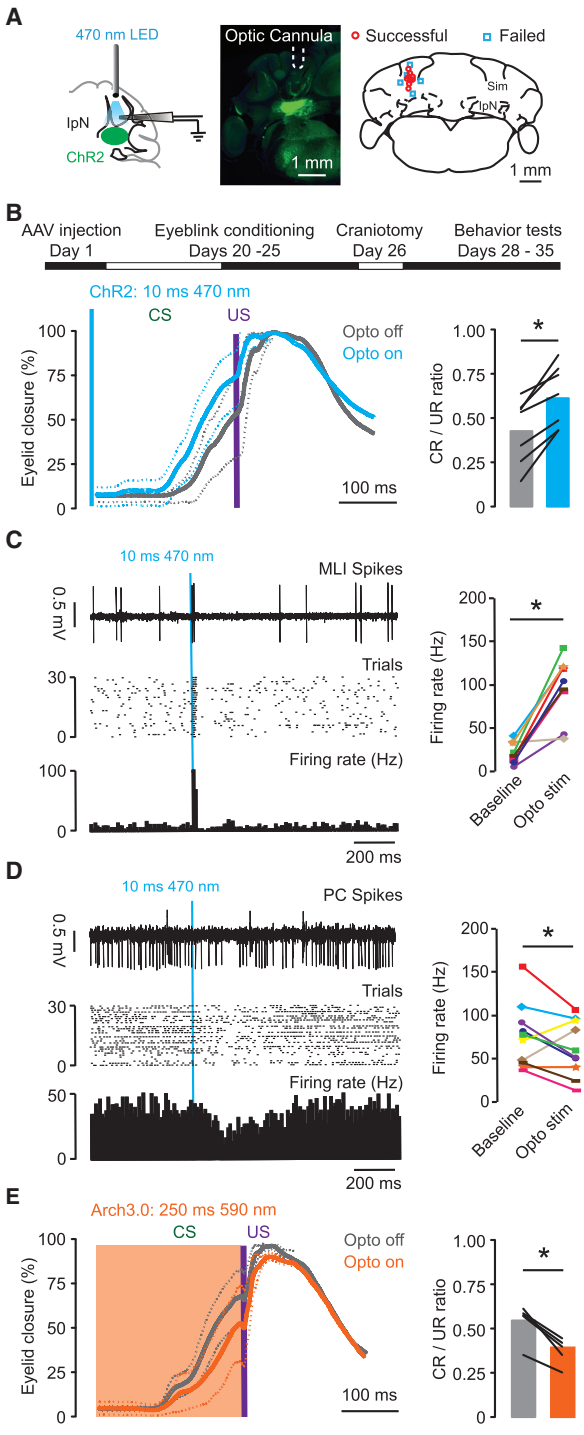

Figure 8. Nucleocortical Pathway Amplifies Amplitudes of Conditioned Eyeblink Response

(A) Panels: (left) Experimental setup of in vivo recording and optogenetic stimulation of the NC-MF in the cerebellar cortex; an example of the location of the optic cannula in the lobule simplex (dashed white line) (middle). (Right) a summary of verified cannula locations in a group of successful and failed experiments.

(B) Experimental setup of optogenetic manipulation during behavioral testing (top). The conditioned eyeblink responses in a trained mouse, in the presence (blue) or absence (gray) of 10 ms optogenetic activation of NC-MF pathway are shown (bottom, left). Optogenetic activation of NC-MF pathways enhances the amplitude of conditioned eyeblink responses in trained mice (bottom, right). CS: conditional stimuli; US: unconditional stimuli; CR: conditioned responses; UR: unconditioned responses.

(C) Optogenetic activation of a MLI. (Top left) a representative trace of increased firing of a MLI in the eyeblink region upon optogenetic activation (10 ms light stimulation is indicated in blue). A raster plot and cumulative histogram of 30 consecutive trials are shown (middle and bottom). (Right) summary of responsive MLI action potential firing upon 10 ms photo-stimulation (n = 9).

(D) Suppression of PC firing following optogenetic stimulation of NC-MFs (left). A representative trace of decreased PC firing upon optogenetic activation is shown (top). A raster plot and cumulative histogram of 30 consecutive trials are shown (bottom, middle). A summary of responsive PCs with both decreased (n = 7) and increased (n = 3) action potential firing upon 10 ms optogenetic stimulation is shown (right).

(E) Conditioned eyeblink responses in a trained mouse expressing eArch3.0, in the presence (orange) or absence (gray) of 250 ms eArch3.0 optogenetic dampening of NC-MF pathway (superimposed with CS) (left). The optogenetic dampening of NC-MF pathways reduces the amplitude of the conditioned eyeblink response in trained mice (right). The data show mean ± SE (*p < 0.05).

Interestingly, the internal and external, excitatory loops may use in part comparable mechanisms within the module(s) involved. Both feedback loops may introduce strong synchronized pauses in PC firing, which in turn can disinhibit CN premotor firing, potentially facilitated by rebound firing and activation by MF and CF collaterals (Bengtsson et al., 2011; De Zeeuw et al., 2011; Hoebeek et al., 2010; Person and Raman, 2012; cf. Alviña et al., 2008).

Given that the internal feedback loop provided by the nucleocortical MF afferents enhances simple spike suppression and that reduced PC activity in turn enhances activity in the cerebellar nuclei neurons, one should consider the possibility that signaling in this loop saturates through internally reinforcing mechanisms (Figure 9). Although some level of reinforcement learning in the cerebellar cortex and nuclei may actually be beneficial for acquisition, consolidation and/or savings of conditioned eyeblink responses (Campolattaro and Freeman, 2009; Medina et al., 2000, 2002), there are several projections in place that might prevent complete saturation. For example, there are also, next to the excitatory internal feedback loop, several types of inhibitory projections from the nuclei to the cerebellar cortex that might operate as an inhibitory internal feedback loop. Indeed, following retrograde tracing of WGA-HRP-colloidal gold complex from the cerebellar cortex to the cerebellar nuclei combined with immuno-cytochemistry, approximately 9% of the retrogradely labeled cells were found to be GABAergic (Batini et al., 1992). In addition, using a viral approach different from the one we applied in the current study, Uusisaari and colleagues recently showed that part of the nucleocortical afferents are glycinergic and selectively inhibit neurograinin-positive Golgi cells, which in turn could enhance granule cell activity (Ankri et al., 2015). To what extent these inhibitory projections provide similar MFs with a similar tendency for structural plasticity during learning and to what extent they can prevent saturation within the excitatory internal feedback remains to be elucidated. However, it is unlikely that they operate in the exact same fashion as the corollary discharge during eyeblink conditioning described in

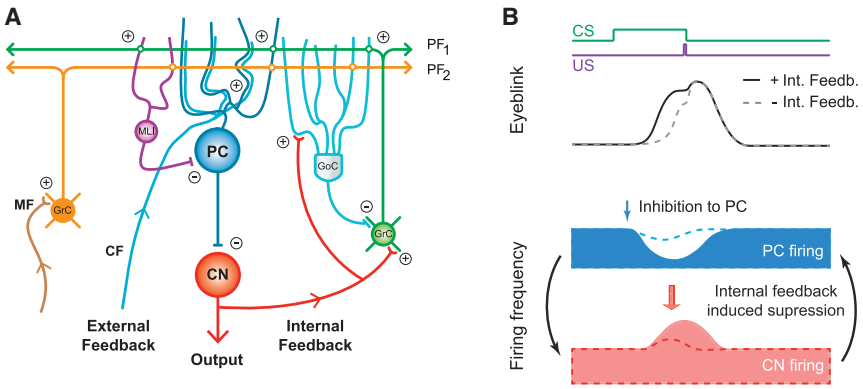

Figure 9. Circuitry and Function of Nucleocortical Circuit

(A) Schematic illustration of a cerebellar nucleocortical circuit in which feedforward and feedbackward circuits co-exist. The feedforward circuit involves mainly pre-cerebellar MF inputs to the cerebellar cortex, whereas the feedbackward circuits entail both a well-known external system mediated by the CFs and an internal system, the function of which is described in the current paper. The excitatory and inhibitory synaptic connections are indicated by "+" and "−," respectively. The GrCs, GoCs, MLI, CN, and PC indicate granule cells, Golgi cells, MLI, cerebellar nuclei neuron, and PC, respectively.

(B) Simplified model indicating how cerebellar cortical firing can be influenced by the nucleocortical loop that mediates the internal feedback. After the onset (blue arrow) of the increased inhibitory input from the MLIs onto the PCs, the firing of CN neurons will increase (red arrow), which in turn will be fed back to neurons in the granular layer (black arrow on the right) further enhancing the interneuron activity and weakening PC firing frequency. As a consequence, such a computational loop leads to a stronger inhibition of PC simple spike firing and higher peak amplitude of firing of cerebellar nuclei neurons (CNs), ultimately resulting in an enhanced eyelid closure. The solid and dashed lines indicate outcomes with and without internal feedback, respectively.

the present study, because they will not mediate an excitatory signal to the mesodiencephalic junction and thus not mediate an efference copy to this area to control premotor activity (De Zeeuw and Ruigrok, 1994). The only inhibitory projection neurons known to leave the cerebellar anlage without targeting the inferior olive are the glycinergic neurons in the medial cerebellar nucleus, which project to vestibular and reticular neurons in the ipsilateral brainstem (Bagnall et al., 2009), i.e., areas unlikely to be involved in eyeblink conditioning (Boele et al., 2010). So, if the inhibitory nucleocortical afferents prevent saturation in the excitatory nucleocortical pathway, they can strictly do so within the internal feedback loop, and not by intervening directly with the corollary discharge at the output level.

Another possible pathway that may provide homeostatic control and thus prevent saturation is formed by the GABAergic fibers that mediate the inhibitory input from the cerebellar nuclei to the inferior olive (Best and Regehr, 2009; Chen et al., 2010; de Zeeuw et al., 1988). When the simple spike activity of the PCs decreases following activation of the excitatory internal feedback loop as described above, the activity of these GABAergic neurons will increase and thus exert a stronger inhibition onto the olivary neurons, which in turn will reduce the CF signals and complex spikes in the PCs within the same olivocerebellar module (De Zeeuw et al., 2011). This reduction in complex spike activity will lead to an increase in simple spike activity, because CF activity induces various forms of short-term and long-term plasticity that will suppress simple spike activity (Gao et al., 2012). Thus, ultimately the initial decrease in simple spike activity leads to a reactive increase in simple spike activity through homeostatic activity in the external olivocerebellar feedback loop, thereby compromising the reinforcing mechanisms in the internal feedback loop that by itself could run into a state of saturation. Interestingly, it is most likely the complex spikes that depend on the GABAergic nucleo-olivary projection that contribute to the moment of onset of the CR (ten Brinke et al., 2015). Thus, this latter homeostatic mechanism appears particularly well designed to prevent the emergence of ill-timed circuits through self-reinforcing processes.

Finally, extra-cerebellar MF systems may also impose strong excitatory inputs to PCs. The morphological and physiological properties of the extra-cerebellar MF inputs are diverse (Chabrol et al., 2015; Palay and Chan-Palay, 1974), and part of these inputs may well convey strong excitatory inputs upon sensorimotor stimulation (Rancz et al., 2007). Thus, in principle, this type of MF may also excite PCs via the granule cell-parallel fiber pathway and counteract the progression of the positive internal feedback.

Together, our findings on the amplifying role of the internal feedback loop provided by the excitatory nucleocortical afferents complement the well-studied olivo-cortico-nuclear modules with a robust and dynamic intra-cerebellar closed-loop architecture that allows reinforcement in a controlled manner. The data imply that feedforward as well as feedback circuitries, the two main architectures of neural computation in the brain, are orchestrated to adaptively control demanding sensorimotor processing.

EXPERIMENTAL PROCEDURES

Here, we provide a summary of the Experimental Procedures; for detailed Experimental Procedures, see Supplemental Experimental Procedures.

Animals

Male and female wild-type mice (C57BL/6) between 3 to 6 months of age were used. All experimental protocols were approved by the institutional animal welfare committee (Erasmus MC).

Stereotaxic Injections

The mice were anesthetized with isoflurane (in O_2). Injections were performed using glass pipettes with mechanical pressure. For AAV injections, 60–120 nl of AAV2-hSyn-ChR2(H134R)-eYFP, AAV2-hSyn-ChR2(H134R)-mCherry, or AAV2-hSyn-eArch3.0-eYFP were pressure injected to the interposed nucleus. For the experiments targeting specifically the anterior IpN, 30–50 nl of AAV was injected. For tracer injections, 20–100 nl BDA 10,000 Da solution and/or fluorescent cholera toxin subunit-B (Ctb Alexa Fluor 488 and Ctb Alexa Fluor 555) were injected to the designated areas. All mice were allowed to recover for >3 days before any subsequent procedure. The mice used for the optogenetic stimulations and extra-cellular recordings were implanted with an optic

cannula, and a craniotomy was placed above the Crus 1 and Crus 2 to access the lobule simplex and the interposed nucleus.

Eyeblink Conditioning Training

We used a green light emitting diode (LED) light as CS. The duration of the CS for all the experiments was kept at 280 ms. The US consisted of a 30 ms air-puff of 30 psi, which co-terminated with the CS. Eyelid position was recorded with a high-speed (250 fps) camera controlled by LabVIEW. The mice were trained for 5 consecutive days.

Optogenetics and Electrophysiology In Vivo

For extra-cellular single-unit recordings, borosilicate glass pipettes filled with 2 M NaCl were positioned stereotactically into the target regions. Brief pulses of 1–10 ms blue light (470 nm) or longer pulses of 250 ms amber light (590 nm) were used to induce the activation or inhibition of nucleocortical MF. Locomotion was monitored using an incremental encoder coupled to the shaft of a cylindrical treadmill. Electrophysiological recordings of cerebellar neurons were acquired with a MultiClamp 700B amplifier (Molecular Devices). All in vivo data were analyzed using SpikeTrain software (Neurasmus BV, Rotterdam, the Netherlands).

Optogenetics and Electrophysiology In Vitro

AAV injected mice were sacrificed >3 weeks post-injection for in vitro experiments. Whole cell and cell attached patch-clamp recordings of nucleocortical MF rosettes, granule cells, Golgi cells, PC, and cerebellar nuclei neurons were performed using differential interference contrast (DIC) and epifluorescence visualization. Patch-clamp recordings were performed using an EPC-10 double amplifier controlled by the PATCHMASTER software (HEKA electronics). Optogenetic stimulation was delivered via the epi-fluorescent light path. To compare the electrophysiological properties of cerebellar neurons between naive and trained mice, we performed patch-clamp recordings in granule cells and PC in a group of mice that underwent eyeblink conditioning (see Experimental Procedures on eyeblink conditioning training).

Immuno-histochemistry and Analysis

Free-floating sections of BDA-stained brains were treated with the avidin-biotin-peroxidase complex method and diaminobenzidine as the chromogen. For immuno-fluorescent staining, free-floating sections were incubated overnight at 4°C with primary antibodies and for 2 hr with fluorescent secondary antibodies. For visualization of the granule and Golgi cell morphology during in vitro electrophysiological recordings, Alexa Fluor 555 or 594 were added to the intracellular solution. For detailed quantification of cerebellar nuclei neuron morphology, biocytin was added to the intracellular solution and visualized with streptavidin Alexa Fluor 488. Images were acquired on an upright LSM 700 confocal microscope (Zeiss) and quantified with FIJI (Schindelin et al., 2012) and Neurolucida software (MBF Bioscience).

Immuno-electron Microscopy

Cerebellar sections of BDA injected mice were cut on a vibratome (Technical Products International) and MF rosettes were visualized by the avidin-biotin-peroxidase complex method. Ultrathin (50–70 nm) sections were mounted on Formvar-coated copper grids. BDA positive MFs were photographed using an electron microscope (Philips) and analyzed using FIJI software.

Statistical Methods

Values are represented as mean ± SE; p values of < 0.05 were considered significant and are reported in the main text. Statistical analysis was done using Student's t test, unless stated otherwise.

SUPPLEMENTAL INFORMATION

Supplemental Information includes Supplemental Experimental Procedures, five figures, and three tables and can be found with this article online at http://dx.doi.org/10.1016/j.neuron.2016.01.008.

AUTHOR CONTRIBUTIONS

Z.G., F.E.H., and C.I.D.Z. conceived and designed the study. Z.G. and M.P.-O. performed experiments; Z.G., M.P.-O., M.M.t.B., Z.L., and T.J.H.R. performed the analyses. Z.G., H.-J.B., and J.-W.P. designed the equipment for behavioral tests. Z.G., F.E.H., and C.I.D.Z. wrote the manuscript with inputs from other authors.

ACKNOWLEDGMENTS

Support was provided by the Netherlands Organization for Scientific Research (NWO)-ALW, MAGW, ZON-MW (Z.G., C.I.D.Z, and F.E.H.); NWO-VENI and EUR-Fellowship (Z.G.); NWO-VIDI (F.E.H.); and Neuro-Basic, ERC-advanced, and ERC-POC (C.I.D.Z.). We thank E. Haasdijk, E. Goedknegt, M. Rutteman, A.C.H.G. Ijpelaar, and K. Voges for technical assistance and K. Kornysheva for constructive discussions.

Received: April 12, 2015
Revised: November 11, 2015
Accepted: December 20, 2015
Published: February 3, 2016

REFERENCES

Ahissar, E., and Kleinfeld, D. (2003). Closed-loop neuronal computations: focus on vibrissa somatosensation in rat. Cereb. Cortex *13*, 53–62.

Aiba, A., Kano, M., Chen, C., Stanton, M.E., Fox, G.D., Herrup, K., Zwingman, T.A., and Tonegawa, S. (1994). Deficient cerebellar long-term depression and impaired motor learning in mGluR1 mutant mice. Cell *79*, 377–388.

Aizenman, C.D., Huang, E.J., and Linden, D.J. (2003). Morphological correlates of intrinsic electrical excitability in neurons of the deep cerebellar nuclei. J. Neurophysiol. *89*, 1738–1747.

Alexander, G.E., DeLong, M.R., and Strick, P.L. (1986). Parallel organization of functionally segregated circuits linking basal ganglia and cortex. Annu. Rev. Neurosci. *9*, 357–381.

Alviña, K., Walter, J.T., Kohn, A., Ellis-Davies, G., and Khodakhah, K. (2008). Questioning the role of rebound firing in the cerebellum. Nat. Neurosci. *11*, 1256–1258.

Ankri, L., Husson, Z., Pietrajtis, K., Proville, R., Léna, C., Yarom, Y., Dieudonné, S., and Uusisaari, M.Y. (2015). A novel inhibitory nucleo-cortical circuit controls cerebellar Golgi cell activity. eLife *4*, 4.

Apps, R., and Hawkes, R. (2009). Cerebellar cortical organization: a one-map hypothesis. Nat. Rev. Neurosci. *10*, 670–681.

Attwell, P.J., Rahman, S., Ivarsson, M., and Yeo, C.H. (1999). Cerebellar cortical AMPA-kainate receptor blockade prevents performance of classically conditioned nictitating membrane responses. J. Neurosci. *19*, RC45.

Badura, A., Schonewille, M., Voges, K., Galliano, E., Renier, N., Gao, Z., Witter, L., Hoebeek, F.E., Chédotal, A., and De Zeeuw, C.I. (2013). Climbing fiber input shapes reciprocity of Purkinje cell firing. Neuron *78*, 700–713.

Bagnall, M.W., Zingg, B., Sakatos, A., Moghadam, S.H., Zeilhofer, H.U., and du Lac, S. (2009). Glycinergic projection neurons of the cerebellum. J. Neurosci. *29*, 10104–10110.

Batini, C., Compoint, C., Buisseret-Delmas, C., Daniel, H., and Guegan, M. (1992). Cerebellar nuclei and the nucleocortical projections in the rat: retrograde tracing coupled to GABA and glutamate immunohistochemistry. J. Comp. Neurol. *315*, 74–84.

Bengtsson, F., Ekerot, C.F., and Jörntell, H. (2011). In vivo analysis of inhibitory synaptic inputs and rebounds in deep cerebellar nuclear neurons. PLoS ONE *6*, e18822.

Best, A.R., and Regehr, W.G. (2009). Inhibitory regulation of electrically coupled neurons in the inferior olive is mediated by asynchronous release of GABA. Neuron *62*, 555–565.

Boele, H.J., Koekkoek, S.K., and De Zeeuw, C.I. (2010). Cerebellar and extracerebellar involvement in mouse eyeblink conditioning: the ACDC model. Front. Cell. Neurosci. *3*, 19.

Boele, H.J., Koekkoek, S.K., De Zeeuw, C.I., and Ruigrok, T.J. (2013). Axonal sprouting and formation of terminals in the adult cerebellum during associative motor learning. J. Neurosci. *33*, 17897–17907.

Campolattaro, M.M., and Freeman, J.H. (2009). Cerebellar inactivation impairs cross modal savings of eyeblink conditioning. Behav. Neurosci. *123*, 292–302.

Casellato, C., Antonietti, A., Garrido, J.A., Ferrigno, G., D'Angelo, E., and Pedrocchi, A. (2015). Distributed cerebellar plasticity implements generalized multiple-scale memory components in real-robot sensorimotor tasks. Front. Comput. Neurosci. *9*, 24.

Cerminara, N.L., and Apps, R. (2011). Behavioural significance of cerebellar modules. Cerebellum *10*, 484–494.

Chabrol, F.P., Arenz, A., Wiechert, M.T., Margrie, T.W., and DiGregorio, D.A. (2015). Synaptic diversity enables temporal coding of coincident multisensory inputs in single neurons. Nat. Neurosci. *18*, 718–727.

Chen, X., Kovalchuk, Y., Adelsberger, H., Henning, H.A., Sausbier, M., Wietzorrek, G., Ruth, P., Yarom, Y., and Konnerth, A. (2010). Disruption of the olivo-cerebellar circuit by Purkinje neuron-specific ablation of BK channels. Proc. Natl. Acad. Sci. USA *107*, 12323–12328.

Crapse, T.B., and Sommer, M.A. (2008). Corollary discharge across the animal kingdom. Nat. Rev. Neurosci. *9*, 587–600.

D'Angelo, E., and De Zeeuw, C.I. (2009). Timing and plasticity in the cerebellum: focus on the granular layer. Trends Neurosci. *32*, 30–40.

De Zeeuw, C.I., and Ruigrok, T.J. (1994). Olivary projecting neurons in the nucleus of Darkschewitsch in the cat receive excitatory monosynaptic input from the cerebellar nuclei. Brain Res. *653*, 345–350.

De Zeeuw, C.I., and ten Brinke, M.M. (2015). Motor learning and the cerebellum. Cold Spring Harb. Perspect. Biol. *7*, a021683.

De Zeeuw, C.I., Hoebeek, F.E., Bosman, L.W., Schonewille, M., Witter, L., and Koekkoek, S.K. (2011). Spatiotemporal firing patterns in the cerebellum. Nat. Rev. Neurosci. *12*, 327–344.

de Zeeuw, C.I., Holstege, J.C., Calkoen, F., Ruigrok, T.J., and Voogd, J. (1988). A new combination of WGA-HRP anterograde tracing and GABA immunocytochemistry applied to afferents of the cat inferior olive at the ultrastructural level. Brain Res. *447*, 369–375.

Dean, P., Porrill, J., Ekerot, C.F., and Jörntell, H. (2010). The cerebellar microcircuit as an adaptive filter: experimental and computational evidence. Nat. Rev. Neurosci. *11*, 30–43.

Dietrichs, E., and Walberg, F. (1980). The cerebellar corticonuclear and nucleocortical projections in the cat as studied with anterograde and retrograde transport of horseradish peroxidase. II. Lobulus simplex, crus I and II. Anat. Embryol. (Berl.) *161*, 83–103.

Gao, Z., van Beugen, B.J., and De Zeeuw, C.I. (2012). Distributed synergistic plasticity and cerebellar learning. Nat. Rev. Neurosci. *13*, 619–635.

Gebre, S.A., Reeber, S.L., and Sillitoe, R.V. (2012). Parasagittal compartmentation of cerebellar mossy fibers as revealed by the patterned expression of vesicular glutamate transporters VGLUT1 and VGLUT2. Brain Struct. Funct. *217*, 165–180.

Gonzalez-Joekes, J., and Schreurs, B.G. (2012). Anatomical characterization of a rabbit cerebellar eyeblink premotor pathway using pseudorabies and identification of a local modulatory network in anterior interpositus. J. Neurosci. *32*, 12472–12487.

Gould, B.B., and Graybiel, A.M. (1976). Afferents to the cerebellar cortex in the cat: evidence for an intrinsic pathway leading from the deep nuclei to the cortex. Brain Res. *110*, 601–611.

Hallett, P.E., and Lightstone, A.D. (1976). Saccadic eye movements towards stimuli triggered by prior saccades. Vision Res. *16*, 99–106.

Hámori, J., Mezey, E., and Szentágothai, J. (1981). Electron microscopic identification of cerebellar nucleo-cortical mossy terminals in the rat. Exp. Brain Res. *44*, 97–100.

Hantman, A.W., and Jessell, T.M. (2010). Clarke's column neurons as the focus of a corticospinal corollary circuit. Nat. Neurosci. *13*, 1233–1239.

Heiney, S.A., Wohl, M.P., Chettih, S.N., Ruffolo, L.I., and Medina, J.F. (2014). Cerebellar-dependent expression of motor learning during eyeblink conditioning in head-fixed mice. J. Neurosci. *34*, 14845–14853.

Hioki, H., Fujiyama, F., Taki, K., Tomioka, R., Furuta, T., Tamamaki, N., and Kaneko, T. (2003). Differential distribution of vesicular glutamate transporters in the rat cerebellar cortex. Neuroscience *117*, 1–6.

Hoebeek, F.E., Witter, L., Ruigrok, T.J., and De Zeeuw, C.I. (2010). Differential olivo-cerebellar cortical control of rebound activity in the cerebellar nuclei. Proc. Natl. Acad. Sci. USA *107*, 8410–8415.

Houck, B.D., and Person, A.L. (2015). Cerebellar premotor output neurons collateralize to innervate the cerebellar cortex. J. Comp. Neurol. *523*, 2254–2271.

Ito, M. (2006). Cerebellar circuitry as a neuronal machine. Prog. Neurobiol. *78*, 272–303.

Ito, M., Yamaguchi, K., Nagao, S., and Yamazaki, T. (2014). Long-term depression as a model of cerebellar plasticity. Prog. Brain Res. *210*, 1–30.

Johansson, F., Jirenhed, D.A., Rasmussen, A., Zucca, R., and Hesslow, G. (2014). Memory trace and timing mechanism localized to cerebellar Purkinje cells. Proc. Natl. Acad. Sci. USA *111*, 14930–14934.

Kalinovsky, A., Boukhtouche, F., Blazeski, R., Bornmann, C., Suzuki, N., Mason, C.A., and Scheiffele, P. (2011). Development of axon-target specificity of ponto-cerebellar afferents. PLoS Biol. *9*, e1001013.

Kelly, R.M., and Strick, P.L. (2003). Cerebellar loops with motor cortex and prefrontal cortex of a nonhuman primate. J. Neurosci. *23*, 8432–8444.

Krupa, D.J., and Thompson, R.F. (1997). Reversible inactivation of the cerebellar interpositus nucleus completely prevents acquisition of the classically conditioned eye-blink response. Learn. Mem. *3*, 545–556.

Llinás, R.R. (2011). Cerebellar motor learning versus cerebellar motor timing: the climbing fibre story. J. Physiol. *589*, 3423–3432.

McCormick, D.A., McGinley, M.J., and Salkoff, D.B. (2015). Brain state dependent activity in the cortex and thalamus. Curr. Opin. Neurobiol. *31*, 133–140.

Medina, J.F., Garcia, K.S., Nores, W.L., Taylor, N.M., and Mauk, M.D. (2000). Timing mechanisms in the cerebellum: testing predictions of a large-scale computer simulation. J. Neurosci. *20*, 5516–5525.

Medina, J.F., Nores, W.L., and Mauk, M.D. (2002). Inhibition of climbing fibres is a signal for the extinction of conditioned eyelid responses. Nature *416*, 330–333.

Morcuende, S., Delgado-Garcia, J.M., and Ugolini, G. (2002). Neuronal premotor networks involved in eyelid responses: retrograde transneuronal tracing with rabies virus from the orbicularis oculi muscle in the rat. J. Neurosci. *22*, 8808–8818.

Moser, E.I., Kropff, E., and Moser, M.B. (2008). Place cells, grid cells, and the brain's spatial representation system. Annu. Rev. Neurosci. *31*, 69–89.

Mostofi, A., Holtzman, T., Grout, A.S., Yeo, C.H., and Edgley, S.A. (2010). Electrophysiological localization of eyeblink-related microzones in rabbit cerebellar cortex. J. Neurosci. *30*, 8920–8934.

Nicolelis, M.A., and Fanselow, E.E. (2002). Thalamocortical optimization of tactile processing according to behavioral state. Nat. Neurosci. *5*, 517–523.

Palay, S.L., and Chan-Palay, V. (1974). Cerebellar Cortex: Cytology and Organization (Springer).

Pennartz, C.M., Berke, J.D., Graybiel, A.M., Ito, R., Lansink, C.S., van der Meer, M., Redish, A.D., Smith, K.S., and Voorn, P. (2009). Corticostriatal interactions during learning, memory processing, and decision making. J. Neurosci. *29*, 12831–12838.

Perrone, J.A., and Krauzlis, R.J. (2008). Vector subtraction using visual and extraretinal motion signals: a new look at efference copy and corollary discharge theories. J. Vis. *8*, 24.1–24.14.

Person, A.L., and Raman, I.M. (2012). Purkinje neuron synchrony elicits time-locked spiking in the cerebellar nuclei. Nature *481*, 502–505.

Pijpers, A., Apps, R., Pardoe, J., Voogd, J., and Ruigrok, T.J. (2006). Precise spatial relationships between mossy fibers and climbing fibers in rat cerebellar cortical zones. J. Neurosci. *26*, 12067–12080.

Rancz, E.A., Ishikawa, T., Duguid, I., Chadderton, P., Mahon, S., and Häusser, M. (2007). High-fidelity transmission of sensory information by single cerebellar mossy fibre boutons. Nature *450*, 1245–1248.

Requarth, T., and Sawtell, N.B. (2014). Plastic corollary discharge predicts sensory consequences of movements in a cerebellum-like circuit. Neuron *82*, 896–907.

Ritzau-Jost, A., Delvendahl, I., Rings, A., Byczkowicz, N., Harada, H., Shigemoto, R., Hirrlinger, J., Eilers, J., and Hallermann, S. (2014). Ultrafast action potentials mediate kilohertz signaling at a central synapse. Neuron *84*, 152–163.

Ruediger, S., Vittori, C., Bednarek, E., Genoud, C., Strata, P., Sacchetti, B., and Caroni, P. (2011). Learning-related feedforward inhibitory connectivity growth required for memory precision. Nature *473*, 514–518.

Ruigrok, T.J., and Teune, T.M. (2014). Collateralization of cerebellar output to functionally distinct brainstem areas. A retrograde, non-fluorescent tracing study in the rat. Front. Syst. Neurosci. *8*, 23.

Rylkova, D., Crank, A.R., Linden, D.J., and Snyder, S.H. (2015). Chronic in vivo imaging of ponto-cerebellar mossy fibers reveals morphological stability during whisker sensory manipulation in the adult rat. eNeuro *2*, http://dx.doi.org/10.1523/ENEURO.0075-15.2015.

Saviane, C., and Silver, R.A. (2006). Fast vesicle reloading and a large pool sustain high bandwidth transmission at a central synapse. Nature *439*, 983–987.

Schindelin, J., Arganda-Carreras, I., Frise, E., Kaynig, V., Longair, M., Pietzsch, T., Preibisch, S., Rueden, C., Saalfeld, S., Schmid, B., et al. (2012). Fiji: an open-source platform for biological-image analysis. Nat. Methods *9*, 676–682.

Schonewille, M., Belmeguenai, A., Koekkoek, S.K., Houtman, S.H., Boele, H.J., van Beugen, B.J., Gao, Z., Badura, A., Ohtsuki, G., Amerika, W.E., et al. (2010). Purkinje cell-specific knockout of the protein phosphatase PP2B impairs potentiation and cerebellar motor learning. Neuron *67*, 618–628.

Schonewille, M., Gao, Z., Boele, H.J., Veloz, M.F., Amerika, W.E., Simek, A.A., De Jeu, M.T., Steinberg, J.P., Takamiya, K., Hoebeek, F.E., et al. (2011). Reevaluating the role of LTD in cerebellar motor learning. Neuron *70*, 43–50.

Shepherd, G.M. (2013). Corticostriatal connectivity and its role in disease. Nat. Rev. Neurosci. *14*, 278–291.

Sommer, M.A., and Wurtz, R.H. (2008). Brain circuits for the internal monitoring of movements. Annu. Rev. Neurosci. *31*, 317–338.

Sperry, R.W. (1950). Neural basis of the spontaneous optokinetic response produced by visual inversion. J. Comp. Physiol. Psychol. *43*, 482–489.

Steuber, V., and Jaeger, D. (2013). Modeling the generation of output by the cerebellar nuclei. Neural Netw. *47*, 112–119.

Strick, P.L., Dum, R.P., and Fiez, J.A. (2009). Cerebellum and nonmotor function. Annu. Rev. Neurosci. *32*, 413–434.

Sugihara, I. (2011). Compartmentalization of the deep cerebellar nuclei based on afferent projections and aldolase C expression. Cerebellum *10*, 449–463.

ten Brinke, M.M., Boele, H.J., Spanke, J.K., Potters, J.W., Kornysheva, K., Wulff, P., IJpelaar, A.C.H.G., Koekkoek, S.K., and De Zeeuw, C.I. (2015). Evolving models of Pavlovian conditioning: cerebellar cortical dynamics in awake behaving mice. Cell Rep. *13*, 1977–1988.

Tolbert, D.L., Bantli, H., and Bloedel, J.R. (1978). Organizational features of the cat and monkey cerebellar nucleocortical projection. J. Comp. Neurol. *182*, 39–56.

Trott, J.R., Apps, R., and Armstrong, D.M. (1998). Zonal organization of cortico-nuclear and nucleo-cortical projections of the paramedian lobule of the cat cerebellum. 1. the C1 zone. Exp. Brain Res. *118*, 298–315.

Umetani, T. (1990). Topographic organization of the cerebellar nucleocortical projection in the albino rat: an autoradiographic orthograde study. Brain Res. *507*, 216–224.

Uusisaari, M., Obata, K., and Knöpfel, T. (2007). Morphological and electrophysiological properties of GABAergic and non-GABAergic cells in the deep cerebellar nuclei. J. Neurophysiol. *97*, 901–911.

Voogd, J., and Ruigrok, T.J. (1997). Transverse and longitudinal patterns in the mammalian cerebellum. Prog. Brain Res. *114*, 21–37.

Voogd, J., and Glickstein, M. (1998). The anatomy of the cerebellum. Trends Neurosci. *21*, 370–375.

Welsh, J.P. (2002). Functional significance of climbing-fiber synchrony: a population coding and behavioral analysis. Ann. N Y Acad. Sci. *978*, 188–204.

Welsh, J.P., Yamaguchi, H., Zeng, X.H., Kojo, M., Nakada, Y., Takagi, A., Sugimori, M., and Llinás, R.R. (2005). Normal motor learning during pharmacological prevention of Purkinje cell long-term depression. Proc. Natl. Acad. Sci. USA *102*, 17166–17171.

Yarom, Y., and Cohen, D. (2002). The olivocerebellar system as a generator of temporal patterns. Ann. N Y Acad. Sci. *978*, 122–134.

Zeilhofer, H.U., Studler, B., Arabadzisz, D., Schweizer, C., Ahmadi, S., Layh, B., Bösl, M.R., and Fritschy, J.M. (2005). Glycinergic neurons expressing enhanced green fluorescent protein in bacterial artificial chromosome transgenic mice. J. Comp. Neurol. *482*, 123–141.

Neuron

Supplemental Information

Excitatory Cerebellar Nucleocortical Circuit Provides Internal Amplification during Associative Conditioning

Zhenyu Gao, Martina Proietti-Onori, Zhanmin Lin, Michiel M. ten Brinke, Henk-Jan Boele, Jan-Willem Potters, Tom J.H. Ruigrok, Freek E. Hoebeek, and Chris I. De Zeeuw

Supplemental Figures

Gao *et al*., Figure S1

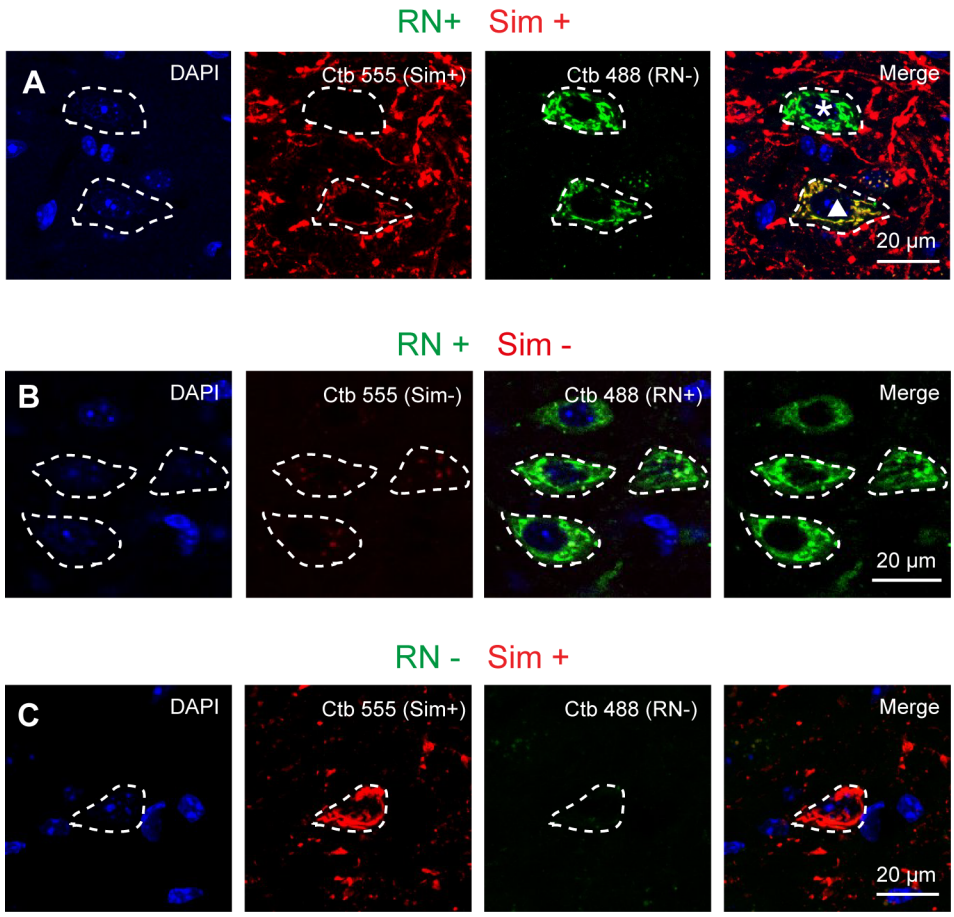

Figure S1. Related to Figure 1. Representative neurons in the IpN with retrograde labeling from red nucleus (RN, Ctb Alexa 488, green) and lobule simplex (Sim, Ctb Alexa 555, red)
(A) Confocal images showing co-labeled IpN neurons (triangle) and a neighboring neuron with RN labeling only (asterisk). (B) Confocal images showing IpN neurons with retrograde labeling from RN only. (C) Confocal images showing an IpN neuron with retrograde labeling from Sim only.

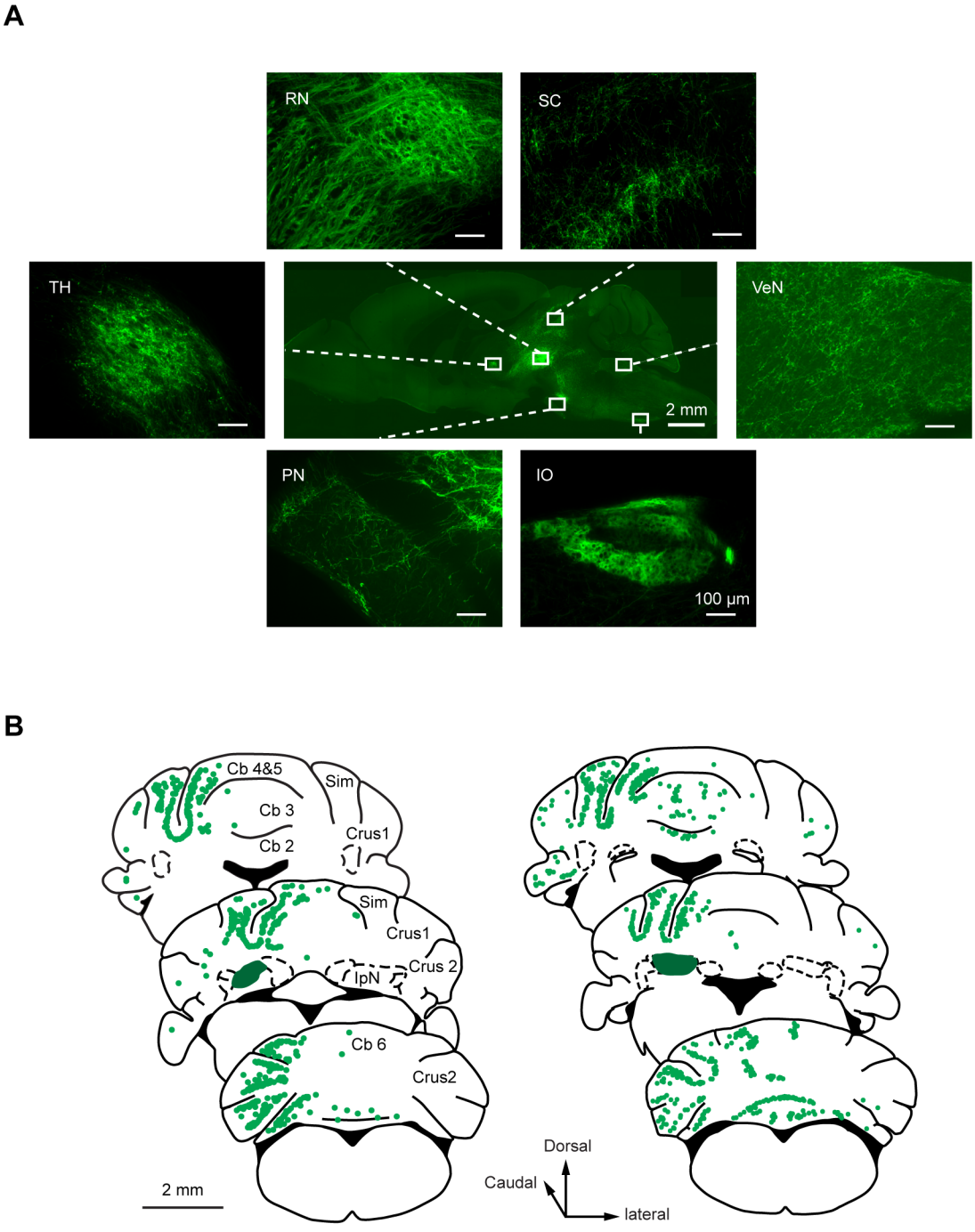

Figure S2. Related to Figure 1. eYFP labeled axonal projections in the IpN targeting regions
(A) Middle: Overview of axonal labeling throughout mouse brain in a sagittal section. Widespread axonal labeling can be found in the mouse in which 100 nl of AAV2-hSyn-hChR2(H134R)-eYFP was injected in the IpN nucleus. Surrounding: High magnification images indicating axonal labeling in the thalamus (TH), red nuclei (RN), superior colliculus (SC), vestibular nuclei (VeN), pontine nuclei (PN) and inferior olive (IO). (B) Representative distribution of nucleocortical MF rosettes in the cerebellar cortex. Schematics show coronal sections from two mice, throughout the regions in which dense nucleocortical MF labeling was observed. The initial IpN injection sites are indicated in dark green contours.

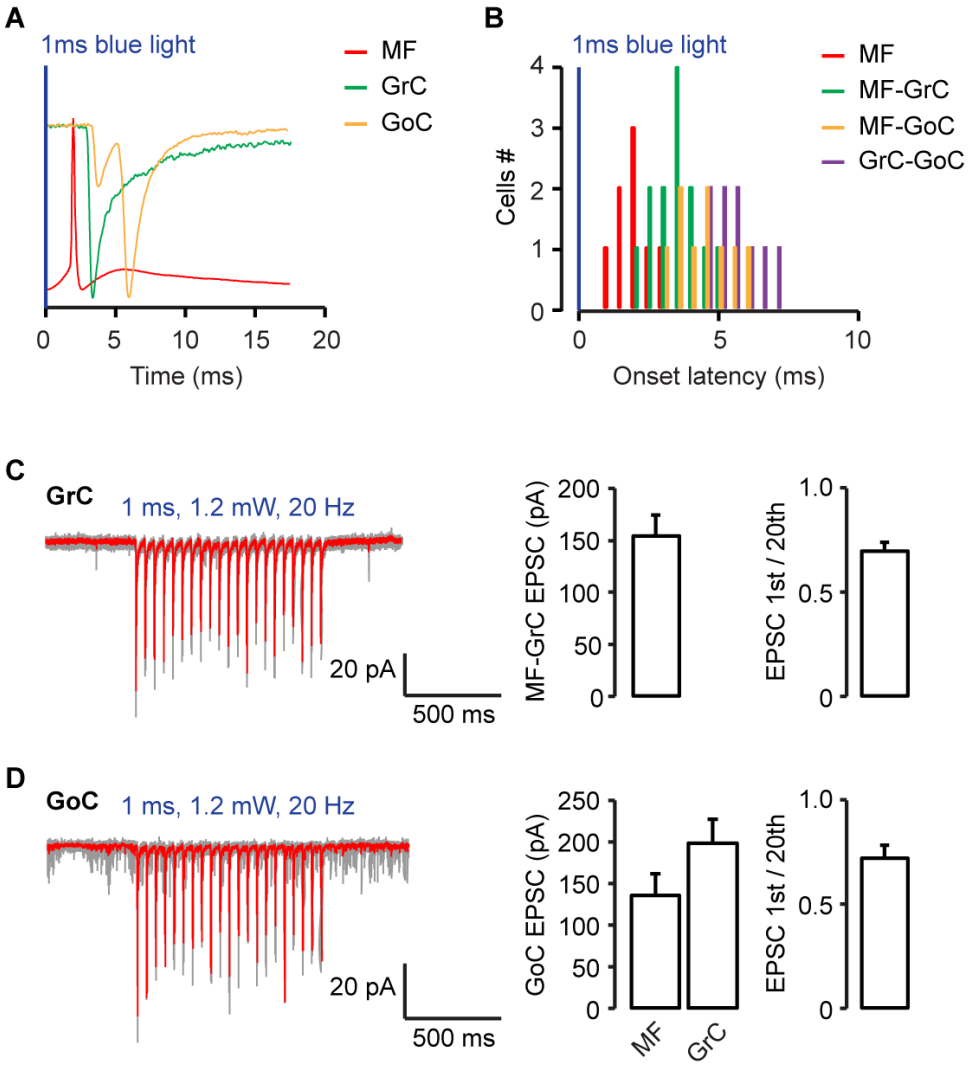

Figure S3. Related to Figure 4. Robust and sustained synaptic transmission between nucleocortical MF and cerebellar cortical neurons

(A) Monosynaptic delay between MF action potential and triggered EPSCs in GrC and GoC. Representative traces of triggered MF action potential, GrC EPSC and GoC EPSC. Traces are normalized for their amplitude and aligned to the start of light pulse. (B) Summary of the onset latency of the nucleocortical MF action potential (n = 10), MF-GrC EPSC (n = 13), MF-GoC and GrC-GoC EPSC (n = 9). (C) Sustained synaptic transmission from nucleocortical MF in response to repetitive stimulation. Left: 5 repetitive traces of MF-GrC EPSCs (gray) and the overlaying averaged trace (red) in response to an optogenetic train stimulation of 20 Hz. Right: summary of first EPSC amplitude and the ratio between the 1st and 20th EPSC during the train stimulation. (D) Similar to (C), left: MF-GoC EPSC in response to an optogenetic train stimulation of 20 Hz. Right: summary of first EPSC amplitude and the ratio between the 1st and 20th EPSC during the train stimulation.

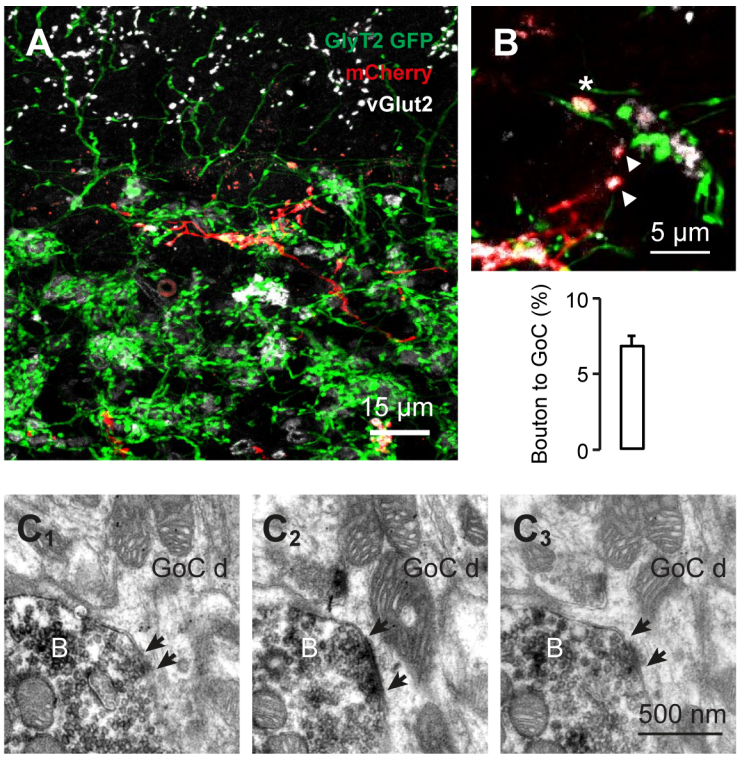

Figure S4. Related to Figure 6. Filopodial boutons form functional synapses with granule and Golgi cells.
(A) Representative image of a nucleocortical MF with filopodia protrusions in the cerebellum of GlyT2-eGFP mice. (B) Inset shows a vGlut2 positive filopodial bouton contacting a GlyT2-GFP positive Golgi cell dendrite (asterisk). Note that the surrounding boutons without contacting Golgi cell dendrites are indicated with arrowheads. Bar chart quantification shows the percentage of vGlut2 positive filopodial boutons that contact Golgi cell dendrites (21 MFs, N = 2). (C) Representative serial EM images of a BDA labeled filopodial bouton with synaptic contacts onto Golgi cell dendrites, as visualized with immunogold labeling. Arrows indicate synaptic contacts.

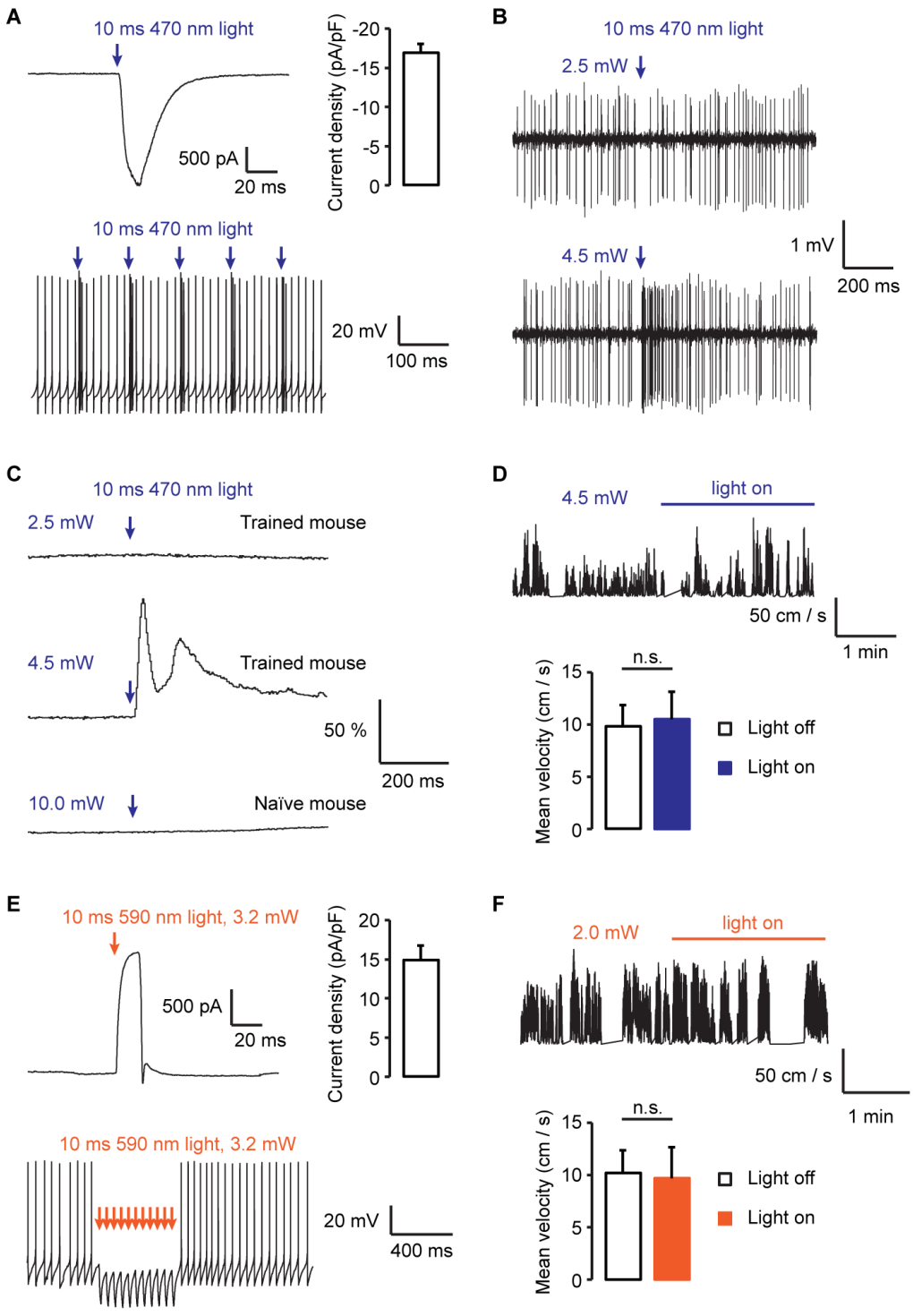

Figure S5. Related to Figure 8. Optogenetic control of nucleocortical activity and behavioral output

(A) Top left: photo current recorded from a ChR2 expressing CN neuron in response to a brief pulse of blue light. Top right: summary of photo current density in ChR2 expressing CN neurons (n = 4). Bottom: example traces showing that five light pulses reliably drive CN cell to fire extra action potentials. (B) Representative CN firing pattern *in vivo*. The optogenetic light intensity was gradually adjusted to probe the threshold for CN neuron direct activation (2.5 mW sub-threshold v.s. 4.5 mW

supra-threshold). For eyeblink conditioning experiments in Figure 8 light intensity was individually adjusted such that it did not exceed the CN activation threshold *in vivo*. (C) Optogenetic stimulation drives eyelid closure. 10 ms 4.5 mW but not 2.5 mW light stimulation directly drives eyelid closure in eyeblink conditioned mouse. Maximum light intensity did not induce detectable eyelid movement in naïve mice. (D) Prolonged subthreshold ChR2 optogenetic stimulation does not affect locomotion on the treadmill. Top: representative traces of running speed with/without optogenetic stimulation; bottom: summary of mean velocity (N = 6). (E) Top left: Photo current from an Arch3.0 expressing CN neuron in response to a brief pulse of amber light. Top right: summary of photo current density in Arch3.0 expressing CN neurons. Bottom: Five light pulses reliably drive CN cell to fire extra action potentials. Note the ChR2 in (A) and Arch3.0 expressing neurons in (E) show similar absolute current densities in our experiments. (F) Prolonged sub-threshold Arch3.0 optogenetic stimulation does not affect locomotion on the treadmill. Top: representative traces of running speed with/without optogenetic stimulation; bottom: summary of mean velocity (N = 5). Data show mean ± s.e., paired student's t-tests.

Supplemental Tables

Gao *et al*., Table S1

Mice	MF counted	MF per area (%)									
									Vermal lobules		
		Fl	PFl	PM	Cop	Crus 1	Crus 2	Sim	1-3	4-6	7-10
1	989	1.6	0.8	3.0	8.9	18.7	9.5	25.7	16.3	5.2	10.3
2	1037	1.0	0.0	0.9	7.2	12.1	3.9	25.8	27.1	17.9	4.1
3	1689	2.5	5.0	2.6	6.9	10.5	11.7	28.0	14.1	10.4	8.2
4	1100	1.2	2.5	3.0	8.9	12.1	15.2	34.2	6.1	12.0	4.9
5	1306	2.5	3.2	1.8	1.8	16.7	10.3	22.9	13.3	12.7	14.8
6	542	3.0	0.7	0.0	6.1	8.5	3.9	31.2	16.1	12.4	18.3
Mean		2.0	2.1	1.9	6.6	13.1	9.1	28.0	15.5	11.8	10.1
SD		0.8	1.9	1.2	2.6	3.9	4.5	4.1	6.8	4.1	5.6

Table S1. Related to Figure 1. Summary of nucleocortical mossy fiber distribution ipsilateral to the IpN injected with AAV vectors.
Fl: flocculus, PFl: paraflocculus, PM: paramedian lobule, Cop: copula pyramidis, Sim: lobule simplex.

Parameter	**NC + (n = 18)** Mean ± s.e.	**NC - (n = 14)** Mean ± s.e.	*t-tests*
Soma size (μm^2)	359.4 ± 45.2	382.7 ± 39.2	0.31
# Primary dendrites	4.2 ± 0.5	4.0 ± 0.3	0.60
Input resistance (MΩ)	145.5 ± 30.4	151.6 ± 25.9	0.47
AP threshold (mV)	-38.2 ± 1.0	-37.4 ± 1.2	0.62
AP amplitude (mV)	44.6 ± 0.8	44.4 ± 1.3	0.68
Rise time (ms)	1.0 ± 0.1	1.1 ± 0.1	0.56
Decay time constant (ms)	2.0 ± 0.8	2.2 ± 0.9	0.58
AP halfwidth (ms)	0.3 ± 0.01	0.3 ± 0.02	0.42
AHP (mV)	-12.5 ± 0.4	-13.3 ± 0.9	0.71

Table S2. Related to Figure 4. Comparisons of electrophysiological properties between identified nucleocortical projecting neurons (NC+) and large CN neurons without detectable nucleocortical axonal projection in the IpN (NC-).

Gao *et al*., Table S3

	Value	n		Value	n
Spontaneous firing rate (Hz)	39.5 ± 6.0	3	AP threshold (mV)	41.3 ± 1.5	7
Resting potential (mV)	-58.3 ± 3.8	7	AP amplitude (mV)	40.4 ± 5.2	7
Input resistance (MΩ)	387.3 ± 29.6	7	Rise time (ms)	0.3 ± 0.1	7
Capacitance (pF)	3.5 ± 1.4	7	Decay time constant (ms)	0.4 ± 0.1	7
Sag ratio	0.5 ± 0.06	7	AP halfwidth (ms)	0.3 ± 0.1	7
1st / 10th AP amplitude ratio	0.81 ± 0.1	7			

Table S3. Related to Figure 5. Summary of the electrophysiological properties of nucleocortical MF rosettes *in vitro*.

Supplemental Experimental Procedures

Animals. Male and female mice (C57BL/6) used for all the experiments were between 3 to 6 months of age and individually housed (food *ad libitum*, 12:12 light/dark cycle). All experimental protocols were approved by the institutional animal welfare committee (Erasmus MC, Rotterdam, The Netherlands).

Stereotaxic injections. Mice were anesthetized with a mixture of isoflurane/oxygen (5% for induction, 1.5-2.0% for maintenance). Rimadyl (5 mg/kg) and buprenorphine (0.05 mg/kg) were applied intraperitoneally 30 mins prior to surgery. Body temperature was monitored and kept constant at 37°C throughout the entire surgical procedure. A patch of skin above the skull was removed and local anesthetic (lidocaine) was topically applied. The skull was prepared with Optibond prime and adhesive (Kerr, Switzerland) and a pedestal was attached with Charisma (Heraeus Kulzer, NY, USA). Mice were then positioned on a custom-made mouse stereotaxic head-holding frame. Small craniotomies (0.2 mm) were made in corresponding sites and injections were performed using glass pipettes (tip opening between 5 and 10 µm) with mechanical pressure. For AAV injections, 60-120 nl of AAV2-hSyn-hChR2(H134R)-eYFP or AAV2-hSyn-eArch3.0-eYFP (10^{12}-10^{13} infectious units per ml, packaged by the UNC Joint Vector Laboratories, RRID: SCR_002448) were injected at a speed of 10 nl/min. For tracer injections, 20-100 nl Biotin Dextran Amine 10 kDa solution (10% w/v in saline, Life Technologies) and fluorescent Cholera toxin subunit-B (Ctb Alexa Fluor 488 and Ctb Alexa Fluor 555, 5% w/v in saline, Life Technologies) were injected at a speed of 10 nl/min. After each injection, the pipette was left in place for >10 minutes before being slowly withdrawn. Coordinates used for injections into the red nucleus were: 0.5 mm to Lambda, 0.5 mm lateral to midline and -4 mm ventral; for injections into the cerebellar lobule simplex: -2.0 mm to Lambda, 2.0 mm lateral to midline and -1.5 mm ventral; for injections into the interposed nucleus: -2.5 mm to Lambda, 2.5 mm lateral to midline and -2.3 mm ventral; for injections into the pontine nucleus: -0.5 mm to Lambda, 0.5 mm lateral to midline and -5.5 mm ventral. All mice were allowed to recover for >3 days before any subsequent procedure. Mice used for the optogenetic stimulations and extracellular recordings were subjected to additional surgery. 2-3 weeks after the virus injection (see above), under the same surgical conditions described above, an optic cannula (400 µm core, 0.39 NA, Thorlabs) was implanted into the lobule simplex with coordinates: -2.0 mm to Lambda, 2.0 mm lateral to midline and -0.5 to -1.0 mm ventral. A craniotomy (1.5 mm in diameter) was placed above Crus 1 and 2 to access the lobule simplex and the interposed nuclei. Antibiotic solution (Baytril 0.5%, Enrofloxacine 5 mg/ml) was applied topically after each experiment.

Eyeblink conditioning training. Head restrained mice were placed on top of a cylindrical treadmill and allowed to walk freely, see also (Heiney et al., 2014). We used a green LED placed 5-10 cm in front of the mouse as conditioned stimulus (CS). The duration of the CS for all the experiments was kept at 280 ms. The unconditional stimulus (US) consisted of an air-puff of 30 psi, 1 cm from the animal's cornea. The onset of the puff was 250 ms after the CS onset (inter-stimulus interval) and the duration was 30 ms, resulting in a co-termination of both stimuli. National Instruments NI-PXI (National Instruments, Austin TX, USA) processor was used to trigger and keep track of stimuli whilst capturing data. Eyelid position was illuminated by infrared LED light and recorded with a 250 fps camera (scA640-120gc, Basler, Ahrensburg, Germany) driven and acquired by custom written routines in LabVIEW. Mice were allowed to habituate on the treadmill for 2 days and followed by acquisition, in which 2 consecutive sessions were presented daily, each session consisting of 100 paired CS–US trials with inter-trial interval (ITI) 5-10 sec. The acquisition sessions were repeated for at least 5 consecutive days.

Optogenetics and electrophysiology *in vivo*. After the behavioral training and the placement of the optic cannula, we extracellularly recorded *in vivo* with or without optogenetic manipulation of the nucleocortical projecting fibers. For extracellular single-unit recordings, borosilicate glass pipettes (OD 1.5 mm, ID 0.86 mm, tip diameter 1-2 µm, Harvard Apparatus, Holliston, MA, USA) filled with 2 M NaCl were positioned stereotactically into the target regions using an electronic pipette micromanipulator (SM7; Luigs & Neumann, Ratingen, Germany). The behavioral responses and the neuronal activity were recorded in response to a brief pulse of light delivered to the brain via an optic fiber coupled with LED light sources (470 nm light for ChR2: M470F1; 590 nm light for eArch3.0 M590F1, Thorlabs). A brief pulse of 1-10 ms blue (470 nm) light or a 250 ms pulse of amber light (590 nm) was used to induce the activation or inhibition of nucleocortical mossy fibers. To avoid direct stimulation of CN soma, we only included data that met all the following criteria: 1) optic cannula were located in the superficial layer of the lobule simplex (see Figure 8A); 2) optogenetic

stimulation/inhibition was adjusted such that no instantaneous increase/decrease of action potential firing in the CN was observed; 3) optogenetic stimulation/inhibition did not result in instantaneous eyeblink responses; and 4) optogenetic stimulation/inhibition did not alter locomotion behavior (Figure S5). Locomotion was monitored using an incremental encoder coupled to the shaft of a cylindrical treadmill (EH30, Eltra, Italy). Purkinje cells were identified by the occurrence of simple spikes and complex spikes and were confirmed to be single unit by the occurrence of climbing fiber pause (Schonewille et al., 2010). Putative molecular layer interneurons were identified as previously described (Badura et al., 2013). CN neurons were identified by their stereotactic location and the characteristic neuronal activity (Hoebeek et al., 2010). Electrophysiological recordings were acquired with a Multiclamp 700B amplifier (Molecular Devices, Sunnyvale, USA) and band-pass filtered at 100-5,000 Hz. Electrophysiological and behavioral data were digitized synchronously using Digidata 1440A (Molecular Devices, Sunnyvale, USA) at 50 kHz. All *in vivo* data were analyzed using SpikeTrain software (Neurasmus BV, Rotterdam, The Netherlands) running under Matlab (Mathworks, MA, USA). Molecular layer interneurons and Purkinje cells were considered responsive if the post-optogenetic-activation firing frequency (measured <200 ms after the offset of light) exceeded 3 times standard deviation of the pre-optogenetic-activation frequency (measured 500 ms before the onset of light).

Optogenetics and electrophysiology *in vitro.* AAV injected mice were sacrificed >3 weeks post injection for *in vitro* experiments. Mice were decapitated under anaesthetized with isoflurane. 300 μm thick cerebellar coronal slices were cut on a vibratome (VT1200s, Leica, Wetzlar, Germany) in ice-cold slicing medium containing (in mM): 240 Sucrose, 5 KCl, 1.25 Na_2HPO_4, 2 $MgSO_4$, 1 $CaCl_2$, 26 $NaHCO_3$ and 10 D-Glucose, bubbled with 95% O_2 and 5% CO_2. Slices were incubated at 34°C for 1 h in the oxygenated ACSF containing (in mM): 124 NaCl, 2.5 KCl, 1.25 Na_2HPO_4, 1 $MgSO_4$, 2 $CaCl_2$, 26 $NaHCO_3$ and 25 D-Glucose and kept at room temperature (21 ± 1 °C) before use. All the experiments were performed with a constant flow of oxygenated ACSF (1.5-2.0 ml/min) at 34 ± 1 °C. Cerebellar neurons were visualized using an upright fluorescent microscope (Axioskop2 FS plus, Carl Zeiss, Jena, Germany) equipped with a 40X water immersion objective. A GFP filter was used to visualize the eYFP labeled mossy fiber terminals. Exposure time to epifuorescent light was kept short to prevent over activation of ChR2 with blue light. Acquired fluorescent images were digitally aligned with the DIC images for identifying eYFP positive mossy fiber rosettes. Whole cell and cell attached patch-clamp recordings of nucleocortical mossy fiber rosettes, granule cells, Golgi cells, Purkinje cells, and cerebellar nuclei neurons were performed under DIC visualization. Patch-clamp recordings were performed using an EPC-10 double amplifier controlled by the Patchmaster software (HEKA electronics, Lambrecht, Germany). All recordings were low-pass filtered at 5 kHz and digitized at 20 kHz. Borosilicate glass pipettes (WPI) were filled with intracellular solution containing the following (in mM): 120 K-gluconate, 9 KCl, 10 KOH, 3.48 $MgCl_2$, 4 NaCl, 10 HEPES, 4 Na_2ATP, 0.4 Na_3GTP and 17.5 sucrose (pH 7.25) and had pipette resistances of 8-10 MΩ for recording mossy fiber rosettes, 4-6 MΩ for recording granule cells and Golgi cells, and 3-4 MΩ for recording Purkinje cells and cerebellar nuclei neurons. Optogenetic stimulation was delivered via the epifluorescent light path. The light intensity was adjusted to 0.1 - 4 mW/mm^2. The light path was controlled by a mechanical shutter (LS2, Vincent Associates, USA). The shutter opening jitter was measured to be 3 ms and was subtracted from all the onset times of the EPSCs driven by optogenetic manipulation. EPSCs in granule and Golgi cells were recorded by holding cells at -70 mV in voltage-clamp mode. Action potential firing was recorded in current-clamp mode without holding current (I = 0). For comparing the inhibition/excitation (I/E) ratios following optogenetic activation of nucleocortical MFs afferents with that of the local electrical activation of a mixed group of MFs, we chose only the Purkinje cells in the lobule simplex that showed clear optogenetically induced EPSCs. For electrical stimulation, a second electrode connected with an Iso-Flex stimulus isolator (A.M.P.I., Jerusalem, Israel) was placed in the white matter adjacent to the recorded Purkinje cells. EPSC and IPSC components were isolated with intracellular solution containing: 120 Cs-gluconate, 10 CsOH, 3.48 $MgCl_2$, 4 NaCl, 10 HEPES, 4 Na_2ATP, 0.4 Na_3GTP and 17.5 sucrose (pH 7.25). EPSCs were acquired at -75 mV, close to the reversal potential of GABAA receptors. The electrical stimulation intensity was adjusted so that the EPSC amplitude was comparable to that of the optogenetic stimulation. The IPSC components were subsequently recorded with holding potential of 0 mV, close to the reversal potential of AMPA receptors. The ratio of the positive peak amplitude at 0 mV and negative peak amplitude at -75 mV was taken as a function of the I/E ratio. To compare the electrophysiological properties of cerebellar neurons between naïve and trained mice, we repeated similar patch clamp recordings in granule cells and Purkinje cells in a group of mice that were fully trained with the eyeblink conditioning paradigm (see eyeblink conditioning section).

Immunohistochemistry and analysis. Mice were deeply anesthetized with an overdose of Nembutal (i.p.) and transcardially perfused with 20 ml saline followed by 50 ml 4% PFA. Brains were extracted and post-fixed overnight in 4% PFA at 4°C. Brains were subsequently embedded in gelatine and cryoprotected in 30% sucrose in PB, frozen on dry ice, and sectioned using a freezing microtome (40 µm thick). For light microscopy analysis of the mice injected with BDA, free-floating sections were blocked for 1h at room temperature in 10% NHS PB solution with 1% triton and visualized with the avidin-biotin-peroxidase complex method (ABC) (Vector Laboratories, Burlingame, USA,) and diaminobenzidine (DAB, 0.05%, Life Technologies) as the chromogen. For immunofluorescent staining, free-floating sections were blocked for 1 h at room temperature in PBS with 0.4% Triton X-100 and 10% NHS solution and incubation 48 hrs at 4°C in a mixture of primary antibodies diluted in PBS with 2% NHS and 0.4% Triton X-100. Sections were then washed and incubated for 2 h at room temperature in a mixture of fluorescent secondary antibodies. Primary antibodies used were rabbit anti-VGlut1 (1:1000, Synaptic Systems, RRID: AB_887876), guinea pig anti-VGlut2 (1:1000, Millipore, RRID: AB_1587626), mouse anti-Calbindin D28K (1:7000, Sigma, RRID: AB_2313712), and goat anti-*Zebrin II* (1:1000, Santa Cruz, RRID: AB_2226594). Slices were then counterstained with DAPI (1:100,000, Invitrogen) and mounted with mounting medium for fluorescence (Vectashield H-1000). All images were acquired on an upright LSM 700 confocal microscope (Carl Zeiss, Jena, Germany) and post-hoc adjusted and analyzed in FIJI software with appropriate plugins (http://pacific.mpi-cbg.de). Ctb labeled neurons were recognized as 'web-like' Golgi apparatus labeling surrounding DAPI labeled cell nuclei, distinct from bouton-like labeling of Purkinje cell axon terminals (Fig. 1). For visualization of the granule and Golgi cell morphology after *in vitro* electrophysiological recordings, Alexa Fluor 555 or 594 (20 µM, Life Technologies) were added to the intracellular solution. For detailed quantification of CN neuron morphology, biocytin (1% w/v) was added to the intracellular solution and visualized with streptavidin Alexa Fluor 488 (1:400, Life Technologies). Immediately after recording, cerebellar slices were fixated in 4% PFA at room temperature for 2-5 hrs, washed in PBS and mounted with mounting medium for fluorescence (Vectashield H-1000). To prevent shrinkage and distortion of thick sections, special care was taken during mounting processes. Cell morphology was acquired on an upright LSM 700 confocal microscope (Carl Zeiss, Jena, Germany) and quantified with FIJI and Neurolucida (MBF bioscience, Williston, USA) software. Nucleocortical projecting IpN neurons were defined following reconstruction of the cell body and axonal projection (see Figure 5). We consider that potential non-nucleocortical projecting neurons are the neurons of which both dendritic tree and axonal projection towards cerebellar peduncle appeared complete, yet no cortical projection was observed.

Immuno-electron microscopy. BDA injected mice were anesthetized with an overdose of nembutal (i.p.) and transcardially perfused with 10 ml saline and subsequently 50 ml 4% PFA and 0.5% glutaraldehyde in cacodylate buffer. Cerebellum was removed and post-fixed overnight in 4% PFA. 80-µm thick coronal sections were cut on a vibratome (Technical Products International, St. Louis, USA). BDA labeled MF rosettes were visualized by incubating the sections with the avidin-biotin-peroxidase complex method (ABC) for 24-48 hrs (Vector Laboratories, USA) and subsequently developed with DAB (0.05%, Life Technologies) as the chromogen. The vibratome sections were rinsed and post-fixed in 1% osmium tetroxide, stained with 1% uranyl acetate, dehydrated and embedded in araldite (Durcupan ACM; Fluka, Buchs, Switzerland). Ultrathin (50-70 nm) sections were cut on an ultramicrotome (Leica, Wetzlar, Germany), mounted on formvar-coated copper grids and contrasted with 2% uranyl acetate and 1% lead citrate (Fluka). For postGABA immunocytochemistry, the grids were rinsed in 0.5 M of Tris buffer with 0.9% NaCl and 0.1% Triton X-100, pH 7.6 (TBST), and incubated overnight at 4ºC in (Sigma, 1:1500 in TBST). The grids were subsequently rinsed twice with TBST and incubated for 1 h at room temperature in goat anti-rabbit IgG labeled with 10 nm gold particles (Aurion) diluted 1:25 in TBST. Cerebellar sections containing BDA positive MFs were photographed using an electron microscope (Philips, Eindhoven, Netherlands). Electron micrographs were analyzed using FIJI software.

Statistical methods. Values are represented as mean ± s.e.; p values of <0.05 were considered significant and are reported in the main text. Statistical analysis was done using student's t-test, unless stated otherwise.

Supplemental References

Badura, A., Schonewille, M., Voges, K., Galliano, E., Renier, N., Gao, Z., Witter, L., Hoebeek, F.E., Chedotal, A., and De Zeeuw, C.I. (2013). Climbing fiber input shapes reciprocity of Purkinje cell firing. Neuron 78, 700-713.

Heiney, S.A., Wohl, M.P., Chettih, S.N., Ruffolo, L.I., and Medina, J.F. (2014). Cerebellar-dependent expression of motor learning during eyeblink conditioning in head-fixed mice. The Journal of neuroscience : the official journal of the Society for Neuroscience 34, 14845-14853.

Hoebeek, F.E., Witter, L., Ruigrok, T.J., and De Zeeuw, C.I. (2010). Differential olivo-cerebellar cortical control of rebound activity in the cerebellar nuclei. Proceedings of the National Academy of Sciences of the United States of America 107, 8410-8415.

Schonewille, M., Belmeguenai, A., Koekkoek, S.K., Houtman, S.H., Boele, H.J., van Beugen, B.J., Gao, Z., Badura, A., Ohtsuki, G., Amerika, W.E*., et al.* (2010). Purkinje cell-specific knockout of the protein phosphatase PP2B impairs potentiation and cerebellar motor learning. Neuron 67, 618-628.